DEUTSCHES ELEKTRONEN-SYNCHROTRON DESY

DESY 88-177
December 1988

Recent Results from PETRA

F. Ould-Saada
II. Inst. f. Experimentalphysik, Univ. Hamburg

ISSN 0418-9833

NOTKESTRASSE 85 · 2 HAMBURG 52

To be sure that your preprints are promptly included in the
HIGH ENERGY PHYSICS INDEX ,
send them to the following address (if possible by air mail) :

DESY
Bibliothek
Notkestrasse 85
2 Hamburg 52
Germany

DESY 88-177
December 1988

ISSN 0418-9833

Recent Results from PETRA

Farid OULD-SAADA
II. Institut für Experimentalphysik
Universität Hamburg

Abstract

A review is given of recent results from the PETRA e^+e^- storage ring. New measurements of the leptonic and hadronic electroweak asymmetries are presented. In the QCD sector, emphasis is placed on jet physics and the determination of the strong coupling constant, α_s. Finally, some results on particle searches, lifetime measurements and 2 γ-physics are reviewed. [1]

[1] Invited talk given at the 1988 Meeting of the DPF of the American Physical Society, University of Connecticut, Stoors, 15-18 August 1988

1 Introduction

Although the PETRA e^+e^- storage ring stopped operating in 1986, interesting physics results are still being produced. This paper reviews some of the recent experimental results. The outline is as follows:

1. In the first section the electroweak asymmetries in both the lepton and quark sectors are discussed
2. In the QCD sector, after discussing multi-jet rates and various α_s determinations, the possibility of experimental observation of the running of α_s is investigated.
3. The third section concerns particle searches. Two examples will be considered: charged Higgs production and neutrino counting.
4. Since the $\tau-$ and $B-$ lifetime measurements have been presented elsewhere, only a summary of the results will be given.
5. Finally, in 2 γ-physics, the status of the η_c and spin 1 resonance production will be considered.

2 Electroweak Asymmetries

The reaction $e^+e^- \to f\bar{f}$ (where f = μ , τ or q) proceeds through the exchange of a photon or a Z^0 boson. The lowest order differential cross-section, taking into account the interference between the photon and Z^0, is given by:

$$\frac{d\sigma}{d\Omega} = \frac{\alpha^2}{4s} \cdot (C_1 \cdot (1 + \cos^2\theta) + C_2 \cdot \cos\theta)$$

where

$$\begin{aligned} C_1 &= Q_f^2 - 2 \cdot Q_f v_e v_f \chi + (v_e^2 + a_e^2) \cdot (v_f^2 + a_f^2) \cdot \chi^2 \\ C_2 &= -4 \cdot Q_f a_e a_f \chi + 8 \cdot v_e v_f a_e a_f \cdot \chi^2 \end{aligned}$$

v_e, v_f, a_e and a_f denote the vector and axial-vector weak couplings of the electron and fermion. In the standard model, a_f and v_f are given by the third component of the weak isospin T_3,

$$a_f = 2(T_{3L} - T_{3R})$$

$$v_f = 2(T_{3L} + T_{3R}) - 4Q_f \sin^2\theta_W$$

where the electroweak mixing angle $\sin^2\theta_W$ determines the neutral current strength. The weak isospin assignments of the standard model are $T_{3L} = -\frac{1}{2}$ and $T_{3R} = 0$.
The forward-backward charge asymmetry in the interference region is given by:

$$A = \frac{N_F - N_B}{N_F + N_B} = \frac{3}{8} \cdot \frac{C_2}{C_1} \approx -\frac{3}{2}\frac{a_e a_f}{Q_f}\chi$$

where N_F is the number of fermions in the forward hemisphere ($\theta \leq 90°$with respect to the e^--beam) and N_B the number of fermions in the backward hemisphere ($\theta \geq 90°$). The approximation is due to neglecting the χ^2 terms which, for leptons, is accurate to one percent

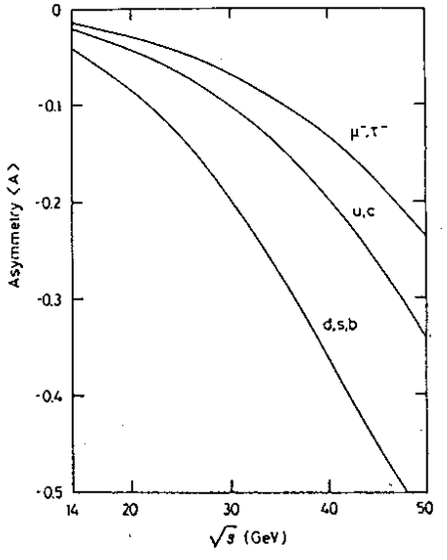

Figure 1: Average asymmetry as a function of the centre of mass energy.

even at the highest PETRA energy. The asymmetry is thus mainly sensitive to the axial weak coupling.

The predicted charge asymmetry is shown in Fig. 1 as a function of the centre of mass energy for the different fermions.

Two parametrizations are currently used to define the propagator term χ:

$$\chi_I = \frac{\rho G_F M_Z^2}{8\pi\alpha\sqrt{2}} \cdot \frac{s}{s - M_Z^2} \quad \text{and} \quad \chi_{II} = \frac{1}{16\sin^2\theta_W \cdot \cos^2\theta_W} \cdot \frac{s}{s - M_Z^2}$$

Parametrization I requires 3 free parameters M_Z, α and the Fermi constant G_F. It has been widely used because α and G_F have been determined accurately. In parameterization II, α, $\sin^2\theta_W$ and M_Z are the free parameters and $\sin^2\theta_W$ is given by $\sin^2\theta_W = 1-(M_W/M_Z)^2$. II is a convenient parameterization because of small one-loop corrections and because it allows a more sensitive determination of $\sin^2\theta_W$ than I. To lowest order the two definitions of χ are the same, they can be transformed into each other using the relations:

$$\rho = \frac{M_W^2}{M_Z^2 \cos^2\theta_W} \quad \text{and} \quad M_W^2 = \frac{\pi\alpha}{\sqrt{2}\, G_F \sin^2\theta_W}$$

with ρ experimentally consistent with 1 within an error of about 2%. Inserting the current numerical parameters [2] results however in different theoretical asymmetry values in parameterizations I and II. This difference is resolved if electroweak one-loop corrections are taken into account.

To compare the data to the theory, we then need to apply the radiative corrections. These can be split into 3 parts:

[2] Unless otherwise stated the following values will be used: α^{-1}=137.036, G_F=1.166 10^{-5} GeV^{-2}, $\sin^2\theta_W$=0.229, M_Z=92.4 GeV.

1. The electromagnetic corrections to the γ exchange (reduced QED correction)
2. The electromagnetic corrections to the Z^0 exchange
3. The purely weak corrections (mainly Z^0 self energy).

At PETRA energies, the reduced QED correction is about 2% for the μ-pair asymmetry. If one uses parametrization II, the corrections 2 and 3 happen to cancel [3]. Therefore, in correcting data, one has to take into account only the reduced QED correction. In the case of parametrization I, the purely weak correction is found to be small [3]. One then has to apply the full QED corrections (1 and 2).

Electroweak interference effects have been extensively studied by the PETRA experiments [1,2].

2.1 Bhabha scattering

For Bhabha scattering the t-channel contributions have to be taken into account. TASSO [4] has measured the differential cross-section of the process $e^+e^- \to e^+e^-$ between 14 GeV and 44 GeV [Fig. 2]. The data agree well with the QED predictions (curves), showing that the effect of Z^0 exchange is small even at the highest PETRA energy. A fit of the high energy data (i.e above 34 GeV) to the standard model yields $\sin^2\theta_W = 0.24 \pm 0.04$. A two parameter fit results in $g_v^2 = -0.08 \pm 0.04$ and $g_a^2 = 0.14 \pm 0.09$. The standard model expectations are 0.0016 and 0.25 respectively. Note that both coupling constants are strongly correlated with a correlation coefficient of 0.5.

2.2 Lepton asymmetries

2.2.1 $e^+e^- \to \mu^+\mu^-$

Some μ-pair angular distributions are shown in Fig. 3 for the PETRA data at 35 GeV. Tab. 1 summarises the PETRA results on the μ-pair asymmetry [1,5]. Also indicated are the PEP [1] and the new TRISTAN results [6].

2.2.2 $e^+e^- \to \tau^+\tau^-$

The JADE collaboration [1] and more recently the CELLO, MARK J and TASSO groups [7] have analysed the τ-pair asymmetry for the 1986 data at 35 GeV, roughly doubling the statistics of their data at this energy. The τ-pair angular distributions are shown in Fig. 4. All the results on the τ-pair asymmetry from PETRA, PEP [1] and TRISTAN [6] are summarized in Tab. 2.

2.3 Quark asymmetries

The forward-backward charge asymmetry of the reactions $e^+e^- \to c\bar{c}$, $e^+e^- \to b\bar{b}$ and $e^+e^- \to q\bar{q}$, where q is any of the 5 known quarks, has been measured by several groups. In case of the c and b quarks, two methods were used to identify the flavour of the heavy quarks: charm quark separation via $D^{*\pm}$ and separation via inclusive leptons.

Table 1: Asymmetries for $e^+e^- \to \mu^+\mu^-$

Experiment	$\sqrt{s}$(GeV)	$\int Ldt$/point(nb^{-1})	Events	$A_{\mu\mu}$ (%)	$A_{St.M}$ (%)
HRS	29	106	5057	$-4.9\pm1.5\pm0.5$	-5.9
MAC	29	226.2	16058	$-5.9\pm0.7\pm0.2$	-5.9
MARK II	29	100	5312	-7.1 ± 1.7	-5.9
AV. PEP	29	432	26427	-5.9 ± 0.62	-5.9
CELLO	34.2	11.3	387	-6.4 ± 6.4	-8.6
CELLO	35.0	92.0	2920	$-8.9\pm2.0\pm1.0$	-8.9
JADE	34.4	71.2	3400	$-11.1\pm1.8\pm1.0$	-8.7
JADE	35.0	92.0	3901	$-10.9\pm1.7\pm1.0$	-8.9
MARK J	34.8	144.3	6854	$-10.4\pm1.3\pm0.5$	-8.7
MARK J	36.4	1.4	65	$-13.6\pm13.5\pm0.5$	-9.7
PLUTO	34.7	44.0	1550	$-13.2\pm2.8\pm1.0$	-8.9
TASSO	34.5	74.7	2673	$-9.1\pm2.3\pm0.5$	-8.6
TASSO	35.0	108.5	2563	$-10.6\pm2.2\pm0.5$	-8.9
AV. PETRA	34.8	277.5	24313	-10.36 ± 0.76	-8.7
CELLO	39.2	12.0	288	$-4.8\pm6.5\pm1.0$	-11.6
JADE	38.0	11.9	422	$-9.7\pm5.0\pm1.0$	-10.8
MARK J	38.3	9.5	403	$-12.3\pm5.3\pm0.5$	-11.0
MARK J	40.4	2.6	87	$+5.0\pm10.5\pm0.5$	-12.5
TASSO	38.3	8.8	173	$+1.7\pm8.6\pm0.5$	-11.0
AV. PETRA	38.6	48.0	1373	-6.99 ± 2.91	-11.2
CELLO	44.0	34.4	611	$-18.8\pm4.5\pm1.0$	-16.2
JADE	43.7	43.1	1258	$-19.1\pm3.1\pm1.0$	-15.6
MARK J	42.0	3.4	116	$-15.9\pm9.3\pm0.5$	-13.8
MARK J	43.8	37.5	1123	$-15.6\pm3.0\pm0.5$	-15.3
MARK J	46.1	5.9	155	$-17.6\pm8.3\pm0.5$	-17.5
TASSO	43.6	35.2	612	$-17.6\pm4.4\pm0.5$	-15.4
AV. PETRA	43.8	160.0	3875	-17.5 ± 1.7	-15.3
AMY	54.5			-28.1 ± 8.7	-28.2
TOPAZ	53.3			-29.2 ± 12.5	-26.4
VENUS	54.3			-32.0 ± 7.0	-27.1
AV.TRISTAN	54.2			-29.22 ± 4.83	-26.8

Table 2: Asymmetries for $e^+e^- \to \tau^+\tau^-$

Experiment	$\sqrt{s}$(GeV)	$\int Ldt$/point(nb^{-1})	Events	$A_{\tau\tau}$ (%)	$A_{St.M}$ (%)
HRS	29	257	7372	$-4.4\pm1.4\pm0.5$	-5.9
MAC	29	210	10153	$-5.5\pm1.2\pm0.5$	-5.9
MARK II	29	100	3714	-4.2 ± 2.0	-5.9
AV. PEP	29	567	21239	-4.9 ± 0.9	-5.9
CELLO	34.2	11.3	434	-10.3 ± 5.2	-8.6
CELLO	35.0	47.5		$-6.5\pm2.5\pm1.5$	-8.9
JADE	34.6	62.4	1998	$-6.0\pm2.5\pm1.0$	-8.8
JADE	35.0	92.4	2900	$-8.5\pm2.0\pm1.0$	-8.9
MARK J	34.7	148.5	1401	$-10.6\pm3.1\pm1.5$	-8.7
PLUTO	34.6	42.3	419	$-5.9\pm6.8^{+0}_{-2.5}$	-8.7
TASSO	34.6	69.4	577	$-4.9\pm5.3^{+1.3}_{-1.2}$	-8.6
TASSO	35.0	108.5	476	$-9.2\pm5.2^{+0.7}_{-3.1}$	-8.9
AV. PETRA	34.8	433.8		-7.69 ± 1.22	-8.7
CELLO	38.1	12.0	260	$-11.8\pm6.2\pm2.7$	-10.9
JADE	38.0	11.8	336	$+7.5\pm6.3\pm1.0$	-10.8
AV. PETRA	38.1	23.8	596	-1.57 ± 4.62	-10.8
CELLO	43.8	21.0	824	$-16.3\pm3.5\pm1.3$	-15.3
JADE	43.7	43.1	913	$-17.0\pm3.6\pm1.0$	-15.3
MARK J	43.8	37.8	287	$-8.5\pm6.6\pm1.5$	-15.3
AV. PETRA	43.8	102.0	2024	-15.56 ± 2.46	-15.3
AMY	54.5			-36.2 ± 10.6	-28.2
TOPAZ	53.3			-20.2 ± 13.5	-26.4
VENUS	54.3			-20.0 ± 11.0	-27.1
AV.TRISTAN	54.2			-25.7 ± 6.4	-26.8

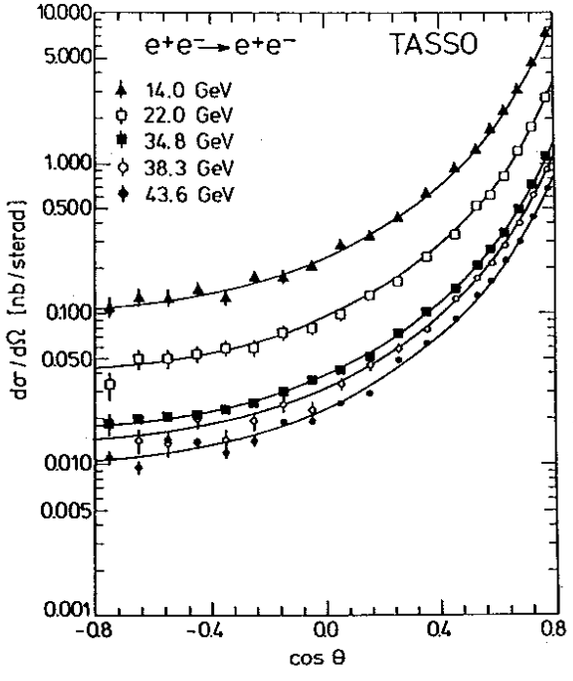

Figure 2: The differential cross-section for the process $e^+e^- \to e^+e^-$ at different energies. Data are from TASSO. The curves show the predictions of QED.

2.3.1 Charm quark separation via $D^{*\pm}$

The charged D^*'s were identified using the decay $D^{*\pm} \to D^0\pi^\pm$. Due to the fact that the Q value of this reaction is only 5.8 MeV, the mass difference $\Delta m = M(D^0\pi) - M(D^0)$ can be measured more accurately than the mass of the $D^{*\pm}$ itself. New results are from JADE and TASSO [8]. The following decay modes of the D^0 were used: $D^0 \to K\pi$,$K\pi(\pi^0)$ and $K\pi\pi\pi$. In order to improve the signal to background ratio, a cut in the $K\pi$,$K\pi(\pi^0)$,$K\pi\pi\pi$ mass spectra was made around the D^0 peak and the energy of the candidate $D^{*\pm}$ was required to be greater than $0.9E_{Beam}$. The Δm distribution from JADE is shown in Fig. 5 in the case where the D^0 decays into $K\pi$. A clear enhancement around $\Delta m = 145\ MeV$ is seen, corresponding to the decay of the $D^{*\pm}$ meson. JADE (resp. TASSO) analysed data at 35 GeV (resp. 35.8 GeV) corresponding to an integrated luminosity of 180pb^{-1}(resp. 234pb^{-1}). The number of $D^{*\pm}$, after background subtraction, is 250 for JADE and 214 for TASSO. The angular distributions are shown in Fig. 6. The preliminary measured charm quark

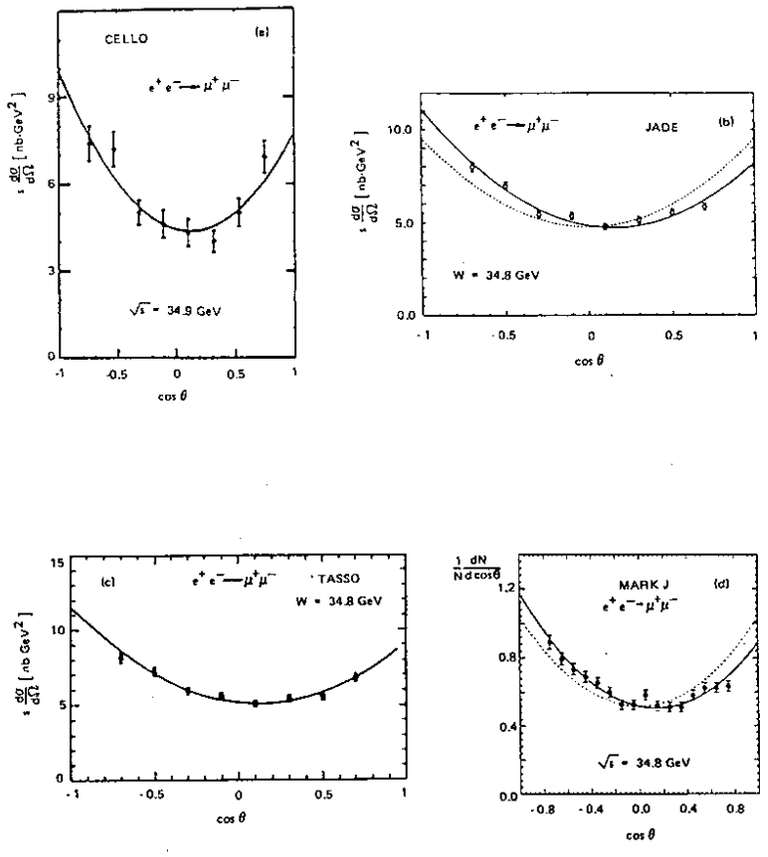

Figure 3: The angular distributions of $e^+e^- \to \mu^+\mu^-$ from the different PETRA experiments. The solid curves represent the electroweak fit. The dotted curves are the QED expectations.

asymmetries: $A_e = (-14.9 \pm 6.7)\%$ (JADE) and $A_e = (-16.6 \pm 7.5)\%$ (TASSO) agree with the previous determinations [Tab. 3] and with the standard model expectation.

2.3.2 Flavour separation via inclusive leptons

Prompt leptons from semileptonic decays provide a unique signature for heavy quark flavour identification. Heavy quarks (b,c) are separated using the transverse momentum of the decay lepton with respect to the jet axis. CELLO [10] has presented new results of their inclusive lepton (e,μ) analysis. The angular distributions of the reactions $e^+e^- \to c\bar{c}$ and $e^+e^- \to b\bar{b}$ are shown in Fig. 7 at 35 GeV and 43GeV. The measured asymmetries are given in Tab. 3 and 4 together with the previous heavy quark asymmetry measurements. The most accurate measurement of the b-asymmetry is that obtained by the JADE group [9].

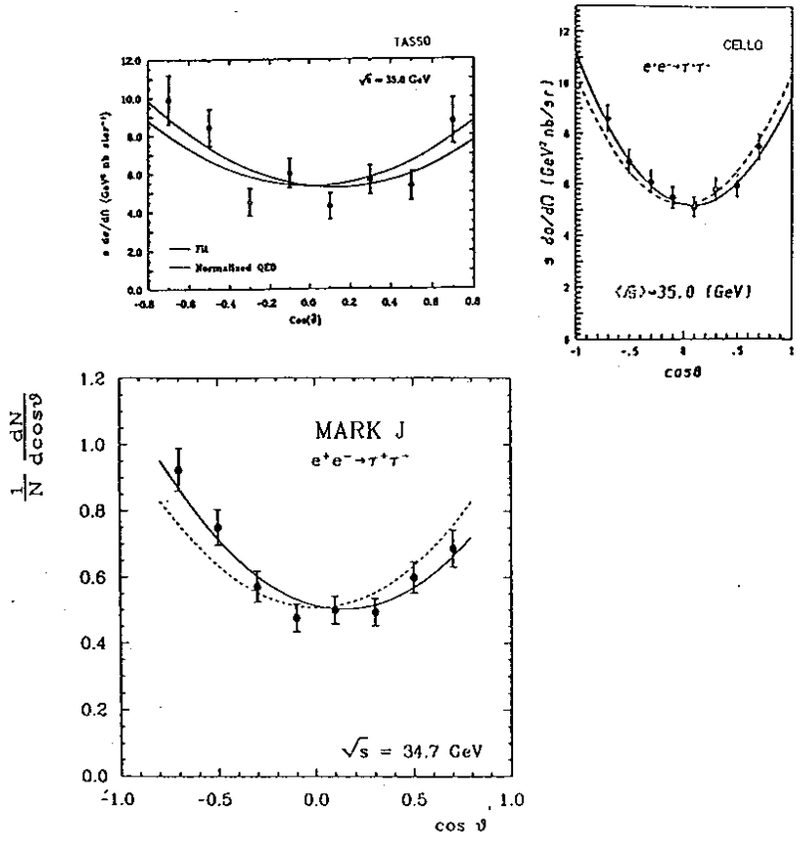

Figure 4: The angular distributions of $e^+e^- \rightarrow \tau^+\tau^-$ from the different PETRA experiments. The solid curves represent the electroweak fit. The dotted curves are the QED expectations.

2.3.3 Jet charge asymmetry

The jet charge asymmetry (averaged over all quark flavours) has been measured by JADE [11] and TASSO [14]. If the quark flavours are produced in the proportions f_d,f_u,f_s,f_c and f_b with the asymmetries A_d,A_u,A_s,A_c and A_b and defining θ to be the angle between the positively charged quark or anti-quark direction and that of the positron, the hadronic asymmetry is then

$$A_h = f_d A_d - f_u A_u + f_s A_s - f_c A_c + f_b A_b$$

the negative sign arising because of the quark charges.

In the JADE analysis, two-jet events were selected by requiring the sphericity to be less than 0.1. The jet charge was determined by defining the Z quantities of the 3 fastest particles

Table 3: Asymmetries for $e^+e^- \rightarrow c\bar{c}$

Experiment	$\sqrt{s}$ (GeV)	Method	A_c (%)	$A_{St.M}$ (%)
HRS	29	D^*	-9.9 ± 2.7	-9.0
TPC	29	e	$-21.0\pm12.0\pm10.0$	-9.0
TPC	29	μ	$-14.0\pm13.0\pm5.0$	-9.0
TPC	29	D^*	-16.0 ± 16.0	-9.0
CELLO	35	e,μ	-8.6 ± 11.0	-13.1
CELLO	43	e,μ	-17.0 ± 19.0	-21.3
JADE	35	D^*	-14.9 ± 6.7	-14.0
MARK J	35.3	μ	-16.0 ± 9.0	-13.9
PLUTO	34.8	μ	-16.0 ± 16.0	-13.4
TASSO	35.8	D^*	-16.6 ± 7.5	-15.7

Table 4: Asymmetries for $e^+e^- \rightarrow b\bar{b}$

Experiment	$\sqrt{s}$ (GeV)	Method	A_b (%)	$A_{St.M}$ (%)
TPC	29	e	$-34.0\pm32.0\pm8.0$	-17.0
TPC	29	μ	$-15.0\pm19.0\pm5.0$	-17.0
CELLO	35	e,μ	-42.0 ± 15.0	-25.3
CELLO	43	e,μ	-18.0 ± 23.0	-38.6
JADE	34.6	μ	$-22.8\pm6.0\pm2.5$	-25.2
MARK J	37	μ	-21.0 ± 19.0	-26.2
PLUTO	34.8	μ	-36.0 ± 25.0	-25.4
TASSO	34.4	e	-25.0 ± 22.0	-24.8
TASSO	34.5	μ	-37.5 ± 27.5	-24.9

in each jet:

$$Z_i = \frac{Q_i P_{Li}}{E_{beam}} \qquad i = 1,2,3$$

where P_{Li} is the momentum component along the sphericity axis and Q_i the charge of the i^{th} particle. To identify the jet charge, a weighting method [12] with the Z_i as the discriminative variables was used. Fig. 8 shows the acceptance corrected angular distribution of the direction of the positive jet, at 34.8 GeV and at 43.8 GeV. The measured asymmetries

$$A_h = 0.060 \pm 0.013 \quad (34.8\ GeV)$$

$$A_h = 0.082 \pm 0.029 \quad (43.6\ GeV)$$

are in agreement with the standard model expectations, including reasonable assumptions concerning the mixing in the $B^0\bar{B}^0$ system [13], of $A_h = 0.050$ and $A_h = 0.085$, respectively. The resulting value of the product of the axial vector coupling constants (including $B^0\bar{B}^0$

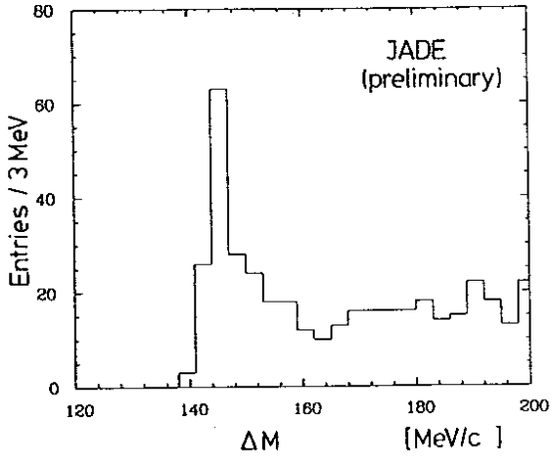

Figure 5: The Δm spectrum measured by JADE for the decay $D^0 \to K\pi$.

mixing)

$$a_e a = -1.09 \pm 0.18 \pm 0.23$$

is in agreement with the standard model value of $a_e a = -1$.

TASSO determined the charge of each jet by using the quantity

$$Q_{jet} = \sum_i q_i x_i^\alpha$$

where the sum runs over the charges q_i of all charged particles of the jet with weights x_i^α. x_i is the ratio of the momentum carried by the i^{th} particle and the reconstructed jet momentum. The value of α is chosen to optimize the charge identification. Monte Carlo studies give $\alpha \sim 0.5$.

The corrected angular distribution of the positive jet for all multihadronic events is shown in Fig. 9. The measured inclusive electroweak asymmetry is

$$A_h = 0.021 \pm 0.005$$

The Monte Carlo simulated events, including electroweak effects, predict $A_h^{sim} = 0.011 \pm 0.004$ ($A_h^{par} = 0.024 \pm 0.004$ at the parton level).

2.3.4 Electroweak fit

All the existing data on the differential lepton cross-sections, the total hadronic cross-sections and the quark asymmetries have been fitted by R. Marshall [15] to extract the elecroweak parameters. The vector and axial-vector lepton couplings for different processes are listed in Tab. 5. Assuming universality, the leptonic data give

$$v^2 = 0.14 \pm 0.06 \quad , \quad a^2 = 1.00 \pm 0.05,$$

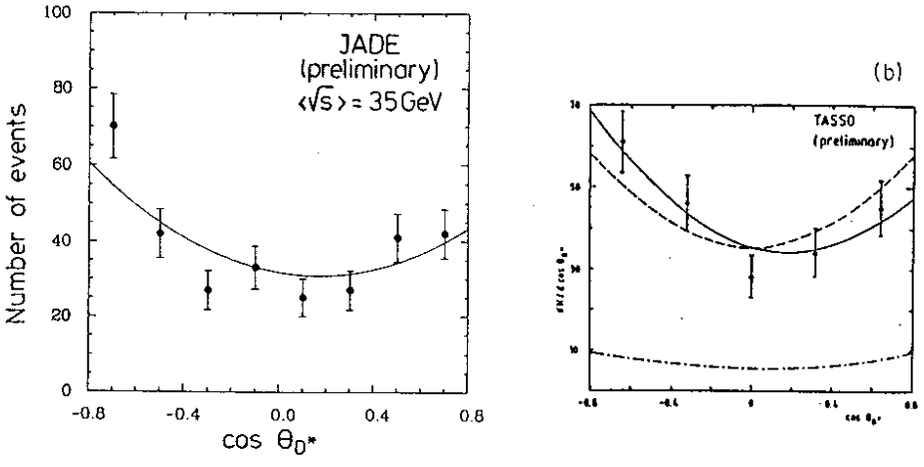

Figure 6: The angular distribution for the process $e^+e^- \to c\bar{c}$ measured via $D^{*\pm}$by a) JADE and b) TASSO.

in good agreement with the standard model expectations of $v^2 = 0.005$ and $a^2 = 1$. Within the standard model, values of $\sin^2\theta_W$ were also obtained [Tab. 5]. The result from the leptonic data is

$$\sin^2\theta_W = 0.222^{+0.015}_{-0.014}$$

For the quark couplings (using the data on the total hadronic cross-sections and the quark asymmetries), R. Marshall obtained the results listed in Tab. 5. The value of $\sin^2\theta_W$ from the hadronic data is $\sin^2\theta_W = 0.241 \pm 0.015$. The combined fit to all data gives:

$$\sin^2\theta_W = 0.232 \pm 0.011 \pm 0.007$$

which agrees with the value measured in ν-experiments [8]

$$\sin^2\theta_W = 0.2309 \pm 0.0029 \pm 0.0024.$$

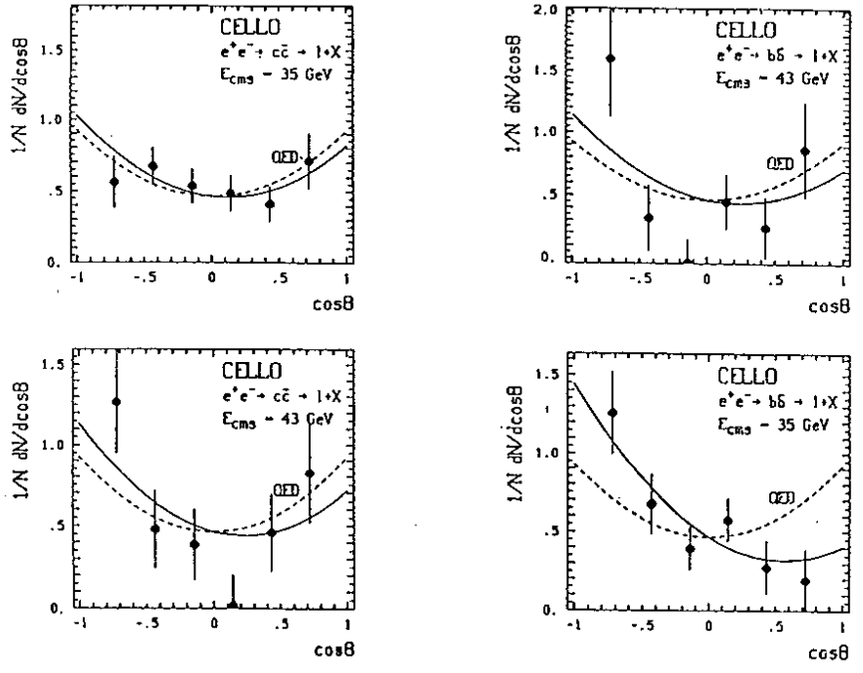

Figure 7: The angular distribution for the reactions $e^+e^- \rightarrow c\bar{c}$ and $e^+e^- \rightarrow b\bar{b}$ from CELLO. The solid curve is the maximum likelihood fit and the broken curve the QED expectation.

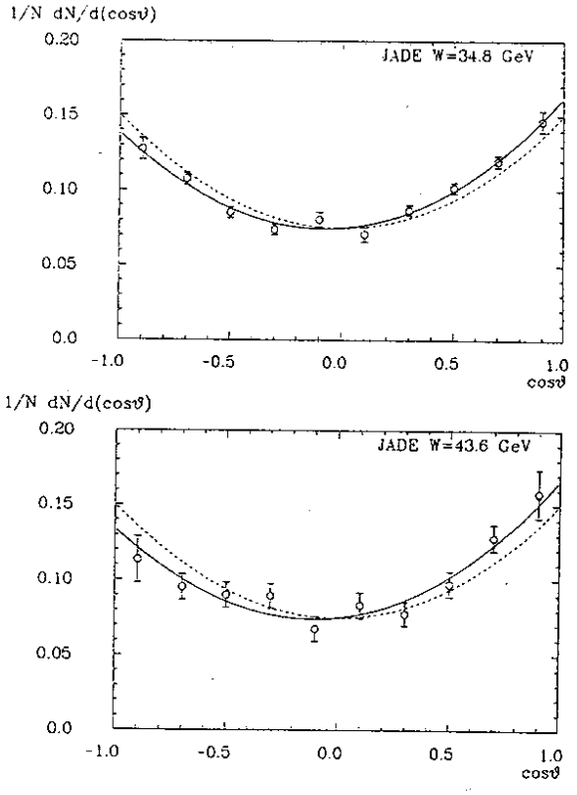

Figure 8: The acceptance corrected angular distribution of the direction of the positive jet, at 34.8 GeV and at 43.6 GeV. The solid curves are fits to the data with asymmetries of 0.060 and 0.082 respectively and the dotted curves are fits with the asymmetry set to zero.

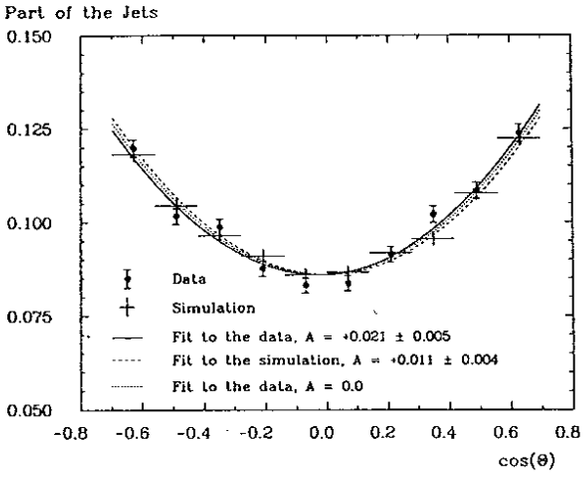

Figure 9: Angular distribution of the positive jet for all multihadronic events from TASSO. The distribution has been corrected for acceptance and radiative effects.

Table 5: Weak coupling constants and $\sin^2\theta_W$

Lepton sector	$v_e v_l$	$a_e a_l$	$\sin^2\theta_W$
e^+e^-	0.13 ± 0.20	1.15 ± 0.31	$0.146^{+0.10}_{-0.03}$
$\mu^+\mu^-$	0.22 ± 0.07	1.00 ± 0.07	$0.181^{+0.015}_{-0.012}$
$\tau^+\tau^-$	-0.04 ± 0.14	0.90 ± 0.10	$0.233^{+0.017}_{-0.016}$
e,μ,τ	0.14 ± 0.06	1.00 ± 0.05	$0.222^{+0.015}_{-0.014}$
Stand Mod $\sin^2\theta_W$=0.23	0.005	+1	
Quark sector	v_q	a_q	$\sin^2\theta_W$
u, c	-0.09 ± 0.75	1.20 ± 0.11	
Stand Mod	+0.38	+1	
			0.241 ± 0.015
d, s, b	-0.36 ± 0.95	-1.06 ± 0.14	
Stand Mod	−0.69	−1	

3 QCD and Jet Physics

In this section, some results on QCD and jet physics are given. The first part concerns multi-jet event rates. Different methods of determining the strong coupling constant α_s are then discussed. Finally, the possibility of experimental observation of the running of α_s is investigated. Results on other topics can be found elsewhere [1,2,16,17,18].

3.1 Multi-jet event rates

The excess of events with large acoplanarity [19], as compared to 2^{nd} order QCD predictions, is related to the underestimate of the rate of 4-jet events, since 3-jet events are planar. It was first pointed out by JADE [19] that the $0(\alpha_s^2)$ models do not reproduce the rate of 4-jet like events [Fig. 10(a)]. The parton shower model, including effects of soft gluon interference [20], describes the observed number of spherical events but underestimates the rate of 3-jet like events.

To define the jet multiplicity of an event, JADE has developed a jet finding algorithm which works as follows: In each event, two particles i and j with the smallest scaled mass $y = M_{ij}^2/E_{vis}^2$ were combined to form one "cluster" by adding the two 4-vectors if y is smaller than a fixed cutoff y_{cut}. This procedure was repeated until all possible combinations of the remaining particles or clusters satisfied the relation $y \geq y_{cut}$ and the resulting number of clusters was called the jet multiplicity of an event. For calculating the scaled mass M_{ij}^2 the expression

$$M_{ij}^2 = 2 \cdot E_i \cdot E_j \cdot (1 - cos\Theta_{ij})$$

was used. The above expression for M_{ij}^2 was chosen in order to obtain the closest agreement between the rates of massive clusters and massless partons at comparable y-values.

TASSO [22], in a similar analysis, found that only the Webber model [20] and the Lund shower model [21] reproduce all jet-rates. Fig. 10(b) shows the n-cluster event rates of the data and different model calculations as a function of y_{cut}.

New results on this subject are given by CELLO [24] and JADE [25]. It was found that the "optimized" 2^{nd} order QCD model is able to describe all the jet rates [3]. "Optimizing" means allowing the renormalization scale parameter μ to vary together with the QCD scale Λ. Traditionally, $\mu^2 = s$ is used in the calculation of cross-sections to absorb terms proportional to $ln(\frac{\mu^2}{s})$ in the running coupling constant. But this choice is not unique [27]. The best agreement between the CELLO data and the "optimized" Lund model, with the GKS second order QCD matrix elements [33], was obtained for $\mu^2 = 0.1\ s$ and $\Lambda_{\overline{MS}} = 80\ MeV$.

Using the ERT QCD second order calculations of jet cross-sections [34], JADE found that all the experimentally observed jet-rates are correctly reproduced for $\mu^2 = 0.005\ s$ and $\Lambda_{\overline{MS}} = 90\ MeV$. Moreover, the use of $\alpha_s(\mu_{opt}^2)$ or $\alpha_s(0.005Q^2)$ instead of $\alpha_s(Q^2)$ gives a good description of all the event structure distributions measured by JADE, except for the P_T^{out} distribution. The fit results are given in Tab. 6 for some variables.

[3] It was pointed out by Kramer and Lampe [23] that if one uses the PMS (Principle of Minimal Sensitivity) criterion [26] to find the optimum scale for the different multijet cross-sections, the 4-jet rate comes out appreciably larger in the 2^{nd} order QCD calculations.

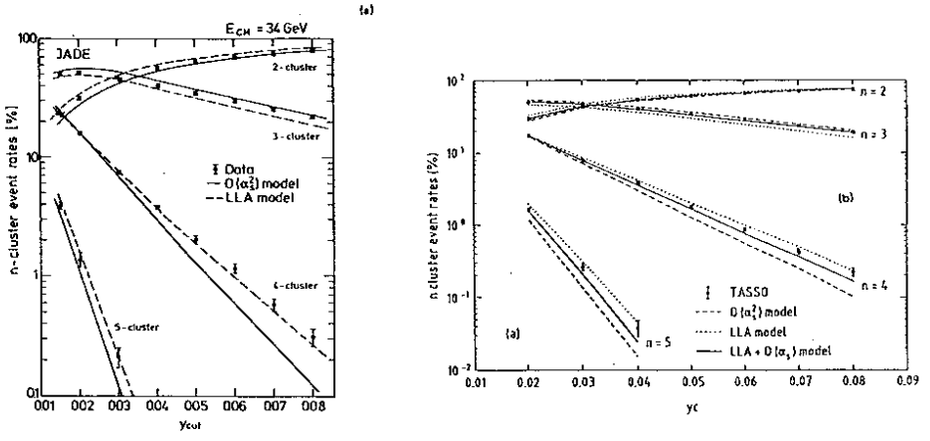

Figure 10: n-cluster event rates of the data and model calculations as a function of y_{cut}, for JADE (a) and TASSO (b).

3.2 α_s measurements

Different methods have been used to measure the strong coupling constant α_s. Some of them will be considered in this section:

- Energy-energy correlation (EEC) and planar triple energy correlation (PTEC),
- Energy dependence of observables,
- Total hadronic cross-section.

3.2.1 α_s from A_{EEC} and P_{TEC}

The energy-energy correlation "EEC" [28], or the energy weighted angular correlation, between final state particles, defined by

$$EEC(\chi) = \frac{1}{N}\sum_{k=1}^{N}\sum_{i,j}\frac{E_i E_j}{s}\delta(\chi - \chi_{ij})$$

where N is the number of events, i and j run over all particles in an event, and χ_{ij} is the angle between particles i and j.

Its asymmetry,

$$AEEC(\chi) = EEC(\pi - \chi) - EEC(\chi),$$

in which fragmentation effects are expected to cancel, may be used to determine α_s. For 2-jet events $EEC(\chi)$ is expected to be symmetric around 90°. Hard gluon emission on the other hand results in a non-vanishing asymmetry. The EEC and the AEEC have been calculated in 2^{nd} order QCD [29,30].

Table 6: JADE data compared to second order QCD model using ERT matrix elements for different scales μ^2

	$\alpha_s(Q^2)$ $\lambda_{\overline{MS}} = 250\ MeV$	$\alpha_s(\mu^2_{opt})$ $\lambda_{\overline{MS}} = 90\ MeV$	$\alpha_s(0.005Q^2)$ $\lambda_{\overline{MS}} = 90\ MeV$
Variable	$\chi^2/d.o.f$	$\chi^2/d.o.f$	$\chi^2/d.o.f$
Acoplanarity	135.1/24	52.7/24	29.5/23
Aplanarity	106.3/27	35.1/24	25.0/25
Thrust	40.7/21	23.4/20	12.1/21
Sphericity	84.8/76	87.7/76	82.0/76
P_T^{out}	418.6/46	367.5/45	329.8/45

The triple energy correlation (TEC) [31] has similar properties to the EEC, except that three particles are considered instead of two. The planar part of the TEC (PTEC) can be used as a new independent quantity for determining α_s.

In a recent analysis, CELLO [32] studied the AEEC and the PTEC in order to measure α_s. The results are shown in Tab. 7 at 35, 38 and 44 GeV. Second order QCD calculations of jet cross-sections from two different groups (GKS [33] and ERT [34]) were used. Different fragmentation models were also considered:

- the string fragmentation model of the LUND group (SF) [36],
- the independent fragmentation of Hoyer et al. (IF0) [37],
- the independent fragmentation of Ali et al. (IF1) [38].

CELLO found that the results do not depend on the QCD calculations of the jet cross-sections. The systematic uncertainties from the choice of the fragmentation model are however large. At 35 GeV, $\alpha_s(SF)/\alpha_s(IF1)$ and $\alpha_s(SF)/\alpha_s(IF0)$ are of the order of 1.2 and 1.5 respectively. The difference between IF0 and IF1 is due to the different treatment of energy and momentum conservation and of the gluon splitting.

All the PEP and PETRA results on α_s from the AEEC [1] are summarized in Fig. 11. The new results (right hand side of Fig. 11) using the Lund fragmentation model with various 2^{nd} order QCD matrix elements of:

- Ellis, Ross and Terrano (ERT) [34],
- Gutbrod, Kramer and Schierholz (GKS) [33],
- Ali and Barreiro (AB) [38],
- Gottschalk and Schatz (GS) [35]

are now in good agreement.

Furthermore, CELLO [32] studied the influence of the renormalization scale μ^2 on $\Lambda_{\overline{MS}}$. The three values of α_s at 35, 38 and 44 GeV were used in a combined fit of the QCD scale parameter $\Lambda_{\overline{MS}}$. With the usual convention $\mu^2 = s$, this resulted in:

$$\Lambda_{\overline{MS}} = (480 \pm 30 \pm 90)\ MeV \qquad (AEEC)$$

Table 7: Results of the determination of α_s from the AEEC and PTEC [CELLO]

Type of Monte Carlo	AEEC 35 GeV	AEEC 38 GeV	AEEC 44 GeV
GKS−SF	0.159±0.003±0.008	0.165±0.009±0.008	0.152±0.005 ±0.006
ERT−SF	0.158±0.003±0.008	0.165±0.009±0.008	0.153±0.005 ±0.006
GKS−IF0	0.104±0.003±0.005		
GKS+IF1	0.127±0.003±0.007		
	PTEC 35 GeV	PTEC 38 GeV	PTEC 44 GeV
GKS−SF	0.154±0.003±0.004	0.148±0.008±0.008	0.145±0.004 ±0.06
ERT+SF	0.151±0.003±0.004	0.146±0.007±0.008	0.143±0.004 +0.06
GKS+IF0	0.106±0.002±0.003		
GKS+IF1	0.128±0.003±0.004		

$$\Lambda_{\overline{MS}} = (380 \pm 30 \pm 60)\ MeV \qquad (PTEC)$$

As shown in Fig. 12, the detemination of $\Lambda_{\overline{MS}}$ from the AEEC at 35 GeV does depend on the relative renormalization scale $x = \frac{\mu^2}{s}$. Λ_{MS} goes down to about 100 MeV at $x = 0.1$ [4].

3.2.2 α_s from the energy dependence of observables

One approach to avoid fragmentation effects in determining α_s is to use the energy dependence of physical quantities. The method was first used by the PLUTO collaboration [39] and R.D. Field [40] and later by JADE [2]. It is based on a direct comparison of 2^{nd} order QCD calculations with the corrected data for physical quantities sensitive to α_s. The energy dependence of an observable O is described as a sum of a QCD term and a fragmentation term $H(s)$:

$$O = C_1\frac{\alpha_s}{\pi}\cdot(1 + C_2(\frac{\alpha_s}{\pi}) + ...) + H(s)$$

The energy dependence of the QCD term follows from the energy dependence of α_s which in the $\overline{MS}$ renormalization scheme is given by:

$$\alpha_s = \frac{2\pi}{b_0 \ln\frac{s}{\Lambda^2_{\overline{MS}}} + \frac{b_1}{b_0}\ln\ln\frac{s}{\Lambda^2_{\overline{MS}}}}$$

where $b_0 = \frac{33-2N_f}{6}$ and $b_1 = \frac{153-19N_f}{6}$ and the number of flavours N_f was set to 5.

CELLO [41] analysed the multihadronic events using this method in order to extract α_s. The variables studied were:

- $1 - T$, where T is the event thrust,

[4] The value of $x = 0.1$ is favoured in order to correctly reproduce the experimentally observed 4-jet rate [see section 2.1].

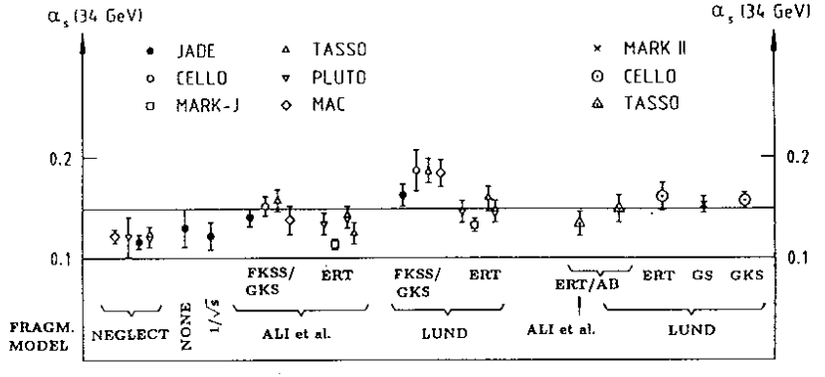

Figure 11: α_s results from e^+e^- experiments using the energy-energy correlation asymmetry.

- M_h^2/s, the heavy jet mass calculated by dividing each event into two hemispheres in such a way that the sum of the two squared invariant masses is minimized,
- $(M_h^2 - M_l^2)/s$, the difference between the jet masses,
- $\int A_{EEC} d\chi$, the integrated asymmetry of the energy-energy correlation.

The results of the 2^{nd} order QCD calculation for the mean values of these variables [42] are given in Tab. 8. The hadronization term $H(s)$ has two important properties. Its magnitude

Table 8: QCD calculations and sign of the hadronization term for some observables

$\langle$	2^{nd} order QCD	H(s)
$1 - T$	$1.05\frac{\alpha_s}{\pi}[1 + 9.05\frac{\alpha_s}{\pi}]$	> 0
M_h^2/s	$1.05\frac{\alpha_s}{\pi}[1 + 6.57\frac{\alpha_s}{\pi}]$	> 0
$(M_h^2 - M_l^2)/s$	$1.05\frac{\alpha_s}{\pi}[1 + 2.76\frac{\alpha_s}{\pi}]$	< 0
$\int A_{EEC} d\chi$	$0.766\frac{\alpha_s}{\pi}[1 + 3.59\frac{\alpha_s}{\pi}]$	< 0

decreases with energy and its sign is always positive for some variables and always negative for others [Tab. 8]. This allows the use of these variables to deduce upper and lower limits for α_s. Fig. 13 shows the corrected CELLO data for $< 1 - T >$, $< M_h^2/s >$, $< (M_h^2 - M_l^2)/s >$

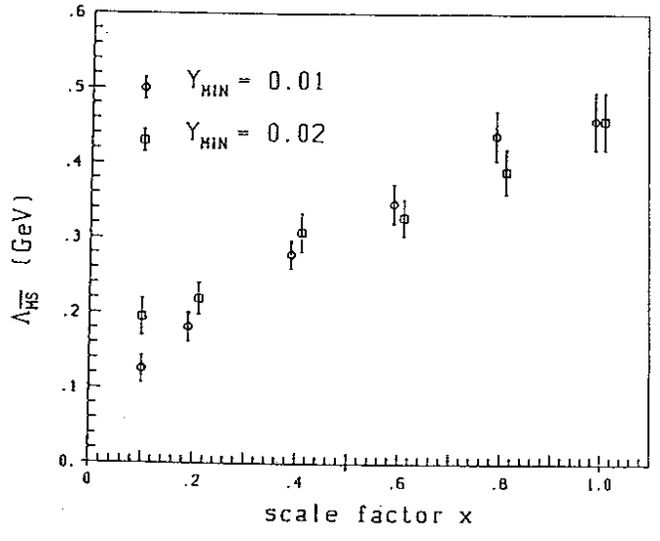

Figure 12: $\Lambda_{\overline{MS}}$ determined from the AEEC at 35 GeV as a function of the relative renormalization scale $x = \mu / \sqrt{s}$ for 2 values of the QCD cut-off parameter Y_{min} [CELLO].

Table 9: 95% confidence limits on $\Lambda_{\overline{MS}}$ and $\alpha_s(35\ \mathrm{GeV})$ from the energy dependence of observables

H(s)	$\Lambda_{\overline{MS}}$(MeV)	$\alpha_s(35\ \mathrm{GeV})$
0	$45 < \Lambda < 655$	$0.107 < \alpha_s < 0.171$
$c/\sqrt{s}$	$56 < \Lambda < 654$	$0.111 < \alpha_s < 0.171$
3^{rd} ord. polyn. in s	$79 < \Lambda < 628$	$0.117 < \alpha_s < 0.169$

and $\int A_{EEC} d\chi$, together with the pure QCD predictions (no hadronization included) for $\Lambda_{\overline{MS}} = 200\ MeV$. It can be seen that for reasonable values of Λ the assumptions about the sign of the hadronization terms for the various observables are valid and that the absolute magnitude of $H(s)$ decreases with energy. The 95% confidence limits on α_s and $\Lambda_{\overline{MS}}$ are summarized in Tab. 9 for different assumptions concerning the hadronization term $H(s)$. The best limits are:

$$79\ MeV < \Lambda_{\overline{MS}} < 628\ MeV$$

$$0.117 < \alpha_s(35\ GeV) < 0.169$$

obtained assuming $H(s)$ to be a 3^{rd} order polynomial in s, subject to the restrictions on sign and monotonous decrease. The lower limit is given by $\int A_{EEC} d\chi$ and the upper limit by $< M_h^2/s >$.

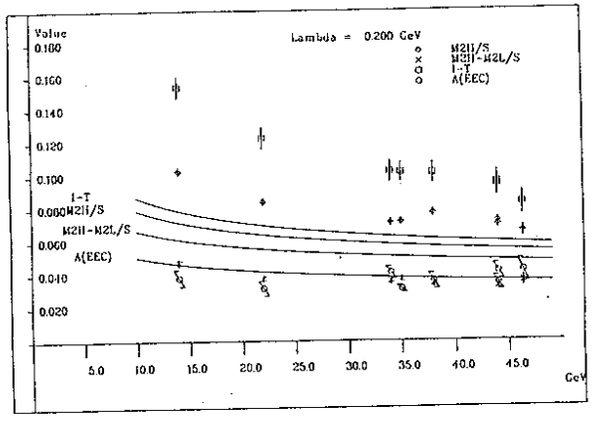

Figure 13: Corrected data for different observables as a function of the center of mass energy from CELLO. The curves correspond to pure QCD predictions (no hadronization included) for $\Lambda_{\overline{MS}} = 200\ MeV$.

3.2.3 α_s from the total hadronic cross-section

The normalized total hadronic cross-section

$$R = \frac{\sigma(e^+e^- \to \gamma, Z_0 \to hadrons)}{\sigma(e^+e^- \to \gamma \to \mu^+\mu^-)}$$

is one of the best quantities to determine the strong coupling constant α_s and the electroweak mixing angle $\sin^2\theta_W$, since it presents no fragmentation dependence and the theoretical uncertainties are small. The main disadvantage is that the QCD contribution to R is small (5% at PETRA energies) and the experimental systematic uncertainties in measuring R are large. CELLO [43] has performed a detailed analysis using all available data on R from PETRA and PEP. The CELLO analysis on R has recently been updated [44]. Data from CESR, DORIS [5] and TRISTAN were included. Also the $0(\alpha_s^3)$ contribution to R has been computed [6] [46] and the higher order QED initial state radiative corrections have been calculated for μ-pair production [47]. Taking into account the new $0(\alpha_s^3)$ contributions, the cross-section ratio reads:

$$R = 3\sum_f \frac{\beta}{2}(3-\beta^2)[1 - C_1^V\frac{\alpha_s}{\pi} + C_2^V(\frac{\alpha_s}{\pi})^2 + C_3^V(\frac{\alpha_s}{\pi})^3]C_{VV}$$
$$+\beta^3[1 + C_1^A\frac{\alpha_s}{\pi} + C_2^A(\frac{\alpha_s}{\pi})^2 + C_3^A(\frac{\alpha_s}{\pi})^3]C_{AA}$$

[5] One has to be careful when including these data because of the transition through the open $b\bar{b}$ threshold [45].
[6] The 3^{rd} order contribution is found to be larger than the 2^{nd} order contribution.

where

$$
\begin{aligned}
C_{VV} &= Q_f^2 - 2\,Q_f v_e v_f\,\chi + (v_e^2 + a_e^2)\,v_f^2\chi^2 \\
C_{AA} &= (v_e^2 + a_e^2)\,a_f^2\,\chi^2 \\
C_2^A &= C_2^V = C_2 = 1.986 - 0.115N^f \\
C_3^A &= C_3^V = C_3 = 70.985 - 1.200N^f - 0.005N_f^2 - 0.840[\frac{(\Sigma Q_f)^2}{\Sigma Q_f}]
\end{aligned}
$$

The propagator term χ and the weak vector and axial-vector coupling constants v_e, v_f, a_e and a_f were defined in section 2. β is the velocity of the quark f of mass m_f, and the functions C_1^V and C_1^A approach 1 when $\beta \to 1$. The running of the strong coupling constant α_s is given by the 3^{rd} order formula [45]:

$$
\alpha_s = \frac{4\pi}{\beta_0 ls}\left(1 - \frac{\beta_1}{\beta_0^2}\frac{log(ls)}{ls} + (\frac{\beta_1}{\beta_0^2})^2\frac{1}{ls^2}\left[(log(ls) - \frac{1}{2})^2 + \frac{\beta_2\beta_0}{\beta_1^2} - \frac{5}{4}\right]\right)
$$

with

$$
\begin{aligned}
ls &= log(\frac{s}{\Lambda^2}) \\
\beta_0 &= 11 - \frac{2}{3}N_f \\
\beta_1 &= 2(51 - \frac{19}{3}N_f) \\
\beta_2 &= \frac{2857}{2} - \frac{5033}{18}N_f + \frac{325}{54}N_f^2.
\end{aligned}
$$

The averaged measured R values are shown in Fig. 14 as a function of $\sqrt{s}$, together with the result of the fit. The fitted values of α_s ($\Lambda_{\overline{MS}}$) are given in Tab. 10 for different energy ranges ($\sin^2\theta_W$ was set to 0.23). Including 3^{rd} order QCD, the value of α_s is $\alpha_s = 0.140\pm0.016$ at 34 GeV. The use of 2^{nd} order QCD calculations instead of 3^{rd} order leads to a systematic increase of α_s by 10% (α_s (34 GeV) = 0.155 ± 0.021). Taking into account higher order QED radiative corrections to R, it was found [44] that α_s is reduced by 4% due to vacuum polarisation and between 0% and 20% due to virtual and hard radiation and for different experimental acceptances.

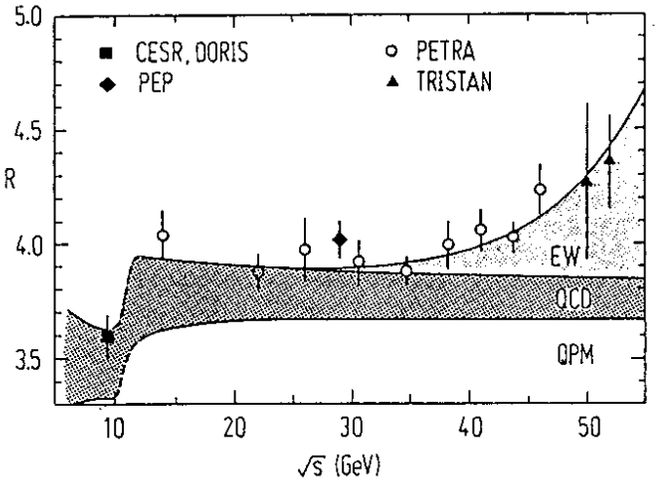

Figure 14: Averaged experimental data on R as a function of the center of mass energy, and best fit using the error matrix for 80 measurements from 16 experiments and setting $\sin^2\theta_W$=0.23.

Table 10: Fitted values from R_{had} of α_s=α_s(34 GeV) and $\Lambda = \Lambda^{(5)}_{\overline{MS}}$ for $\sin^2\theta_W$=0.23

Data	Energy range	$0(\alpha_s^2)$	$0(\alpha_s^3)$
PEP, PETRA	14 - 47 GeV	α_s=0.169±0.025 $\Lambda = 610^{+470}_{-340} MeV$	α_s=0.151±0.019 $\Lambda = 320^{+240}_{-180} MeV$
PEP, PETRA TRISTAN	14 - 52 GeV	α_s=0.167±0.025 $\Lambda = 580^{+460}_{-330} MeV$	α_s=0.149±0.019 $\Lambda = 310^{+230}_{-170} MeV$
CESR, DORIS, PEP, PETRA, TRISTAN	7 - 52 GeV	α_s=0.155±0.021 $\Lambda = 400^{+300}_{-220} MeV$	α_s=0.140±0.016 $\Lambda = 220^{+150}_{-120} MeV$

3.3 Is α_s running?

Some methods of determining the strong coupling constant α_s were presented in the previous section and many other measurements have been carried out in the past few years. However, the energy dependence of α_s has not yet been established. This is a crucial test of QCD, since it is related to the asymptotic freedom of the theory. Furthermore, from the degree of energy dependence, it is possible to extract the QCD scale parameter $\Lambda_{\overline{MS}}$.

The JADE collaboration [48] has investigated the energy dependence of α_s by studying the evolution of the fraction of 3-jet events produced $R_3 = \frac{\sigma_{3-jet}}{\sigma_{tot}}$, where σ_{tot} is the total hadronic cross-section and σ_{3-jet} is the corresponding 3-jet cross-section, between 22 GeV and 44 GeV.

Second order perturbative QCD predicts that

$$R_3 = C_1 \cdot \alpha_s + C_2 \cdot \alpha_s^2.$$

Within a particular renormalization scheme, the coefficients C_1 and C_2 are functions of the jet resolution parameter y_{cut} but do not depend on the centre of mass energy. As a resolution criterium, one can use the scaled invariant mass of 2 partons i and j: $y_{ij} = \frac{M_{ij}^2}{E_{CM}^2}$. A cut-off parameter y_{min} ($y_{ij} \geq y_{min}$) defines the number of resolvable partons. Experimentally, it is possible to adopt this as a jet finding algorithm (see section 3.1). For a fixed y_{min}, the energy dependence of α_s is only given by the behaviour of R_3. To compare the experiment with the theory, however, one has to check that no energy dependence is introduced by the jet finding algorithm and the corrections applied to the data. The overall correction is found to be 1 within 2%. Fig. 15(a) shows the ratio

$$q = \frac{R_3(rec.\ jets)}{R_3(partons)}$$

as function of the centre of mass energy for $y_{cut} = y_{min} = 0.08$, using model calculations. For $E_{CM} \geq 28\ GeV$, the ratio q is constant and close to 1. This is valid for $y_{cut} = 0.04$ - 0.14. The increase of q for lower energies is due to non-perturbative effects: decays of heavy particles and fragmentation. One may then compare the number of experimentally observable jets directly with QCD. The results are presented in Fig. 15(b), where the 3-jet rate R_3 is shown as a function of E_{CM} for different y_{cut} values. The points represent the data and the curves show pure QCD 2^{nd} order calculations by Gottschalk and Schatz [35] and by Kramer and Lampe [23]. For $y_{cut} \geq 0.04$, direct QCD calculations describe both the energy dependence of the data and the absolute normalization. For $E_{CM} \geq 30\ GeV$, the QCD prediction gives a χ^2 of 1/d.o.f, whereas the α_s = constant model gives a χ^2 of 4/d.o.f. This can be translated into a 4σ effect in favour of the running of α_s.

Another consistency check is to study the ratio, r, of 3-jet rates, $r = \frac{R_3(E)}{R_3(E')}$ at 2 different energies. QCD predicts $r < 1$ for $E > E'$. Fig. 15(c) shows r for the data at $E = 44\ GeV$ and $E' = 34.6\ GeV$, together with the QCD $0(\alpha_s^2)$ predictions of Kramer and Lampe for three different values of $\Lambda_{\overline{MS}}$. For $y_{cut} > 0.04$, the ratio r is lower than 1 and is independent of y_{cut}, which is consistent with α_s decreasing with increasing energy.

From the energy dependence of r, it is possible to determine $\Lambda_{\overline{MS}}$. Averaging r in the region of $y_{cut} > 0.04$ results in a mean value of $< r > = 0.935 \pm 0.023$. This corresponds, if compared to the 2^{nd} order QCD calculations of Kramer and Lampe, to

$$\Lambda_{\overline{MS}} = (450^{+700}_{-370})\ MeV$$

$$\alpha_s(44\ GeV) = 0.154 \pm 0.038$$

Note that this determination is independent of fragmentation models.

A similar analysis was performed by the TASSO collaboration [22], using the same method of jet reconstruction. Fig. 16(a) shows the ratio r of 3-jet rates, $r = \frac{R_3(W)}{R_3(35\ GeV)}$ for the data at W=14, 22 and 43.8 GeV. The ratio does not depend on y_{cut} for W=43.8 GeV. r increases for W=14 and 22 GeV due to fragmentation effects. The 3-jet rate R_3 is presented in Fig. 16(b) for data at 22, 35 and 43.8 GeV and for Monte Carlo at W>50 GeV. The TASSO data are compatible with a running α_s (full curve). The dotted curve corresponds to a model with a constant $\alpha_s = 0.265$.

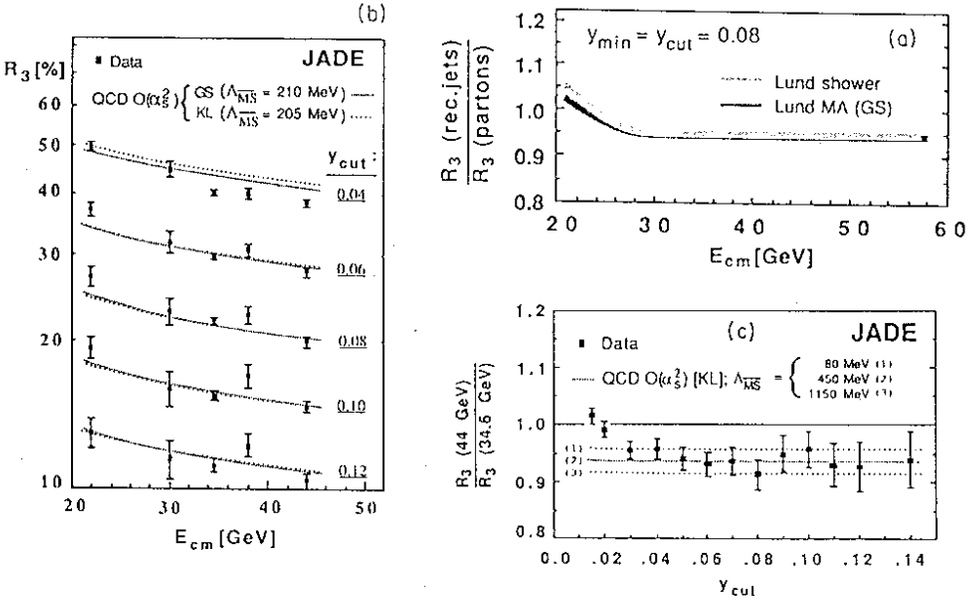

Figure 15: (a) The ratio q of reconstructed 3-jet and 3-parton event rates for different QCD and fragmentation model calculations. (b) 3-jet event rates at different centre of mass energies for various values of y_{cut}, together with the predictions of the complete 2^{nd} order QCD calculations of Gottschalk and Schatz and of Kramer and Lampe. (c) The ratio of 3-jet event rates observed at E_{cm} = 44 GeV and 34.6 GeV.

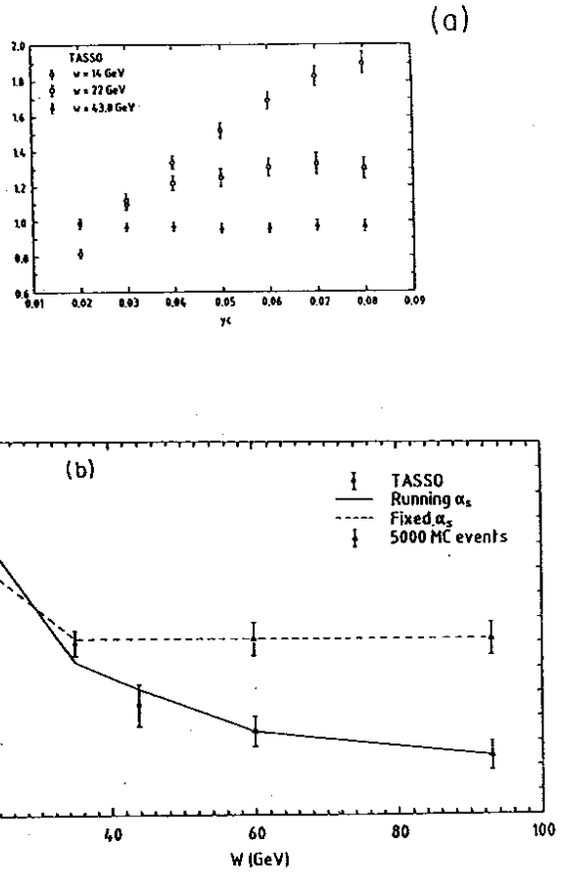

Figure 16: (a) The ratios $\frac{R_3(14)}{R_3(35)}$, $\frac{R_3(22)}{R_3(35)}$ and $\frac{R_3(44)}{R_3(35)}$, for the data as a function of y_{cut}. (b) R_3 defined by $y_{cut} = 0.08$ as a function of the center of mass energy for the data and $LLA + 0(\alpha_s)$ model with both a running α_s and a constant α_s.

4 Particle Searches

Two examples of particle searches will be considered in this section: the search for charged scalar particles and neutrino counting.

4.1 Search for Charged Scalar Particles

The minimal Standard Model requires one Higgs scalār doublet corresponding to one physical particle, the neutral Higgs boson H^0. The existence of charged scalar particles ($H^{\pm}$) is predicted in a number of models, e.g. supersymmetry, technicolor models or electroweak models with a non-minimal Higgs sector. The differential cross-section for the process $e^+e^- \rightarrow H^+H^-$ is given by:

$$\frac{d\sigma}{d\Omega}(e^+e^- \rightarrow H^+H^-) = \frac{\alpha^2}{8s}\beta^3 sin^2\theta$$

where $\beta = \sqrt{1 - \frac{m_H^2}{s}}$ is the Higgs velocity and θ is the polar angle with respect to the beam axis. Various PETRA experiments [49] already presented results in 1982. Charged Higgs particles were assumed to decay predominantly into heavy particles:

$$H^+ \rightarrow c\bar{s}\ ,\ c\bar{b}\ ,\ \tau^+\nu_\tau$$

with the experimental signatures: acoplanar τ-pairs, acoplanar τ-jet or 4-jet events.

JADE and CELLO [50] updated their previous searches last year. Recently, TASSO [51] extended their original search by analysing the highest energy data sample , 40 GeV< $\sqrt{s}$< 47 GeV , which corresponds to an integrated luminosity of 34 pb^{-1}. The decay mode $H^+H^- \rightarrow 4-jets$ was considered. The 95% confidence limits for the hadronic branching ratios vs. the Higgs mass are presented in Fig. 17 for the following assumptions concerning the branching ratios: $(c\bar{s}) = 1$ (a), $(c\bar{b}) = 1$ (b) and $(c\bar{s}):(c\bar{b}) = 1{:}1$ (c). The CELLO and JADE results are shown in Fig. 18.

The PETRA experiments exclude charged Higgs with masses from 3.5 GeV to 19 GeV, independent of the hadronic and leptonic branching ratios.

4.2 Neutrino Counting

A search for single photons, produced in e^+e^-collisions together with particles interacting only weakly with matter, has been performed by the CELLO collaboration [52]. It has been suggested [53] that the reaction $e^+e^- \rightarrow \nu\bar{\nu}\gamma$ can be used to tag the process $Z_0 \rightarrow \nu\bar{\nu}$, and hence to count the number of light neutrino species N_ν. The cross-section for the process $e^+e^- \rightarrow \nu\bar{\nu}\gamma$, assuming massless neutrinos, reads [54]:

$$\frac{d\sigma(e^+e^- \rightarrow \nu\bar{\nu}\gamma)}{dxdy} = \frac{2\alpha}{\pi}\frac{s(1-x)}{x(1-y^2)}[(1-\frac{x}{2})^2 + x^2\frac{y^2}{4}]\sigma(e^+e^- \rightarrow \nu\bar{\nu})$$

$$\sigma(e^+e^- \rightarrow \nu\bar{\nu}) = \frac{G_F^2}{6\pi}[2 + \frac{N_\nu(v_e^2 + a_e^2) + 2(v_e + a_e)(1 - \frac{s(1-x)}{m_Z^2})}{(1 - \frac{s(1-x)}{m_Z^2})^2 + \frac{\Gamma_Z^2}{m_Z^2}}]$$

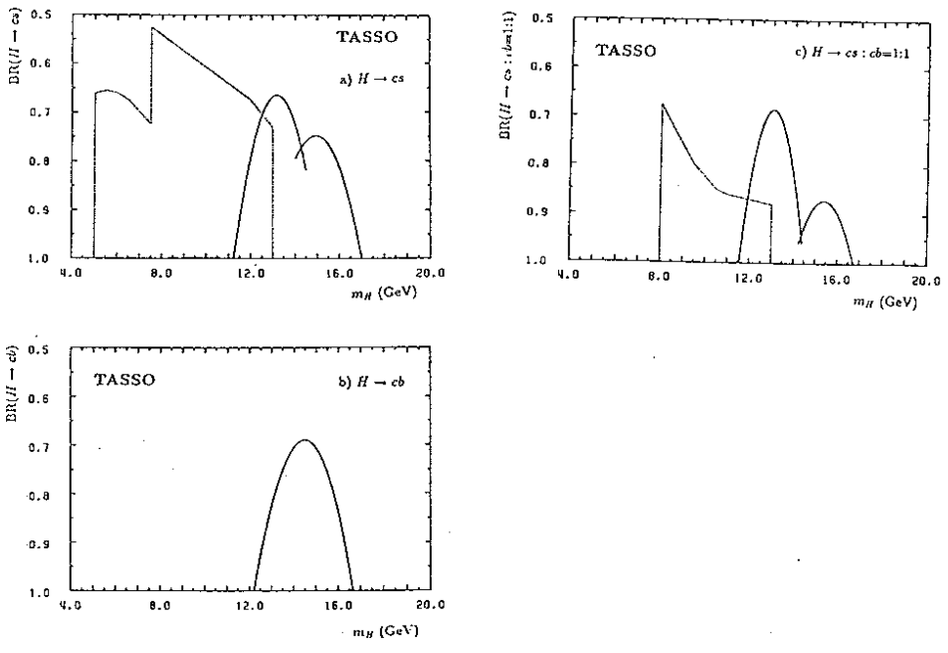

Figure 17: 95% CL upper limits on the (a) $c\bar{s}$, (b) $c\bar{b}$ and (c) $c\bar{s} : c\bar{b} = 1 : 1$ decay branching ratios for the process $e^+e^- \to H^+H^-$ as a function of the Higgs mass

where x is the energy of the photon divided by the beam energy, $\sqrt{s}$ is the center of mass energy, $y = cos\theta$, θ is the polar angle of the photon with respect to the beam axis, v_e and a_e are the vector and axial-vector couplings of the electron and Γ_Z is the total width of the Z_0. If a decay into 3 charged leptons, 6 quarks and N_ν neutrinos is assumed, then:

$$\Gamma_Z = \frac{M_Z^3 G_F}{12\pi\sqrt{2}}[21 + N_\nu - 48\sin^2\theta_W + 64 sin^4\theta_W]$$

To avoid the important background from the QED process $e^+e^- \to e^+e^-\gamma$, hard kinematical cuts on the transverse photon energy $E_T^\gamma = E_\gamma sin\theta_\gamma$ and on θ_γ were necessary. CELLO results are presented in Tab. 11 at 2 different energies, together with the MARK J results [55]. CELLO observed 1.26 events where 1.87 were expected. They put the limit $N_\nu < 8.7$ at 90% CL. CELLO combined results from PEP [56] and PETRA. The 90 and 95% CL limits on the number of neutrinos N_ν and on the number of additional neutrinos ΔN_ν are shown in Tab. 12, together with the $p\bar{p}$ results [57].

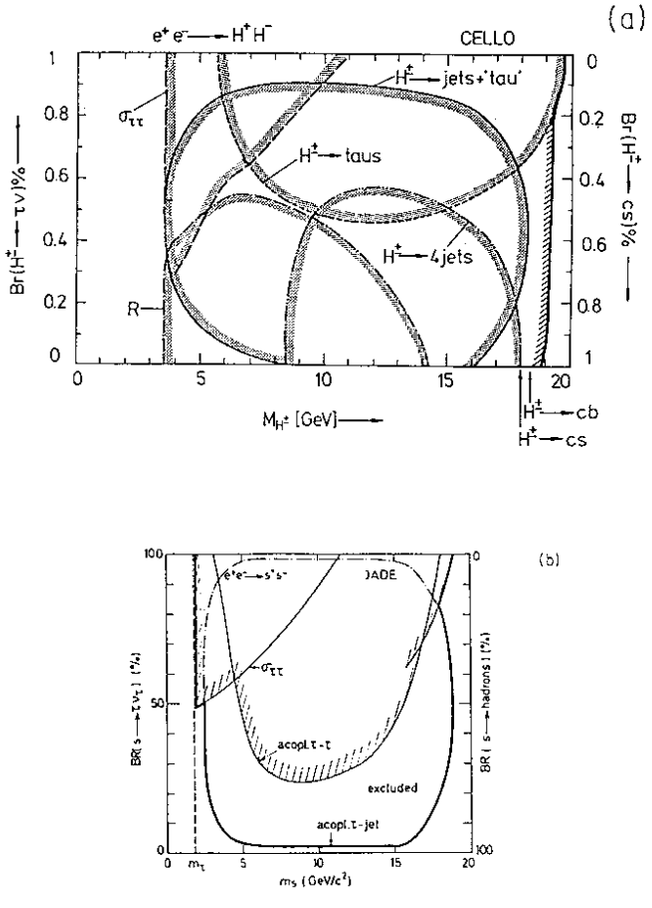

Figure 18: 95% CL limits on the mass of a charged scalar Higgs decaying into τ's or hadrons from CELLO (a) and JADE (b).

Table 11: 90% CL limits on the number of neutrinos

Search	$\sqrt{s}$ [GeV]	acceptance cuts	acceptance %	$\int Ldt$ [pb^{-1}]	expected yield	observed yield	N_ν
CELLO 1	42.6	$E_{T_\gamma} > 2.13 GeV$ $\theta_\gamma > 20^\circ$	0.4	37.6	0.66	1.26	<8.7
CELLO 2	35.0	$E_{T_\gamma} > 1.75 GeV$ $\theta_\gamma > 34^\circ$	0.5	85.0	1.21		
MARK J	39.0	$E_{T_\gamma} > 3.90 GeV$ $\theta_\gamma > 20^\circ$	0.3	35.5	0.39	0	<26

Table 12: Summary on the number of neutrinos obtained by e^+e^- and $p\bar{p}$ experiments

Experiment	N_ν 90 (95)% CL	ΔN_ν 90 (95)% CL	N_ν (central value)
CELLO	<8.7 (11.3)	<8.2 (10.9)	$1.3^{+6.7}_{-1.2}$
e^+e^- CELLO+MARKJ ASP+MAC	<4.6 (5.8)	<3.7 (4.7)	$1.0^{+2.9}_{-1.0}$
$p\bar{p}$ (UA1+UA2)	<5.7	<2.9	$1.8^{+2.0}_{-1.5}\pm0.6$ (m_t=44GeV)
			$-0.1^{+1.7}_{-1.3}\pm0.6$ (m_t=80GeV)

5 Lifetime Measurements

In this section, only a summary of the τ- and B-lifetimes will be given, since these have been presented in other contributions to this conference. Tab. 13 summarises new measurements of the τ lifetime by CELLO, JADE and TASSO [58], together with measurements from other experiments [61]. The world average is

$$\tau_\tau = 0.303 \pm 0.008 \; psec.$$

The results of the B-lifetime measurements are summarized in Tab. 14. Also listed are the $b\bar{b}$ enrichment method used and the quantity measured. New PETRA measurements are from JADE and TASSO [59]. A recent preliminary result from JADE [60] ($1.32^{+0.29}_{-0.26}$) has been added to the table presented at the Munich conference [61]. The world average is [7]

$$\tau_B = 1.15 \pm 0.14 \; psec.$$

[7] This does not include the recent JADE result.

Table 13: Summary of τ lifetime measurements

Experiment	τ_τ (ps)
CLEO	0.325 ± 0.023
ARGUS	0.295 ± 0.018
DELCO	$0.300^{+0.050}_{-0.040}$
HRS	0.299 ± 0.018
MAC	0.309 ± 0.019
MARKII	0.288 ± 0.023
CELLO	$0.470^{+0.390}_{-0.290}$
JADE	0.301 ± 0.029
TASSO	0.306 ± 0.024
Average	0.303 ± 0.008

Table 14: Summary of B-lifetime measurements

Experiment	$b\bar{b}$ event enrichment	Measured quantity	τ_B (ps)
DELCO	High P_T Lepton	Lepton Impact Param.	$1.17^{+0.27\ +0.17}_{-0.22\ -0.16}$
HRS			$1.02^{+0.41}_{-0.37}$
JADE			$1.80^{+0.50}_{-0.40} \pm 0.40$
JADE			$1.32^{+0.29}_{-0.26}$
MARKII			$0.98 \pm 0.12 \pm 0.13$
MAC	High P_T Lepton	Hadron Impact Param.	$1.29 \pm 0.20 \pm 0.21$
TASSO	Boost. Spher. Prod.	Hadron Impact Param.	$1.36 \pm 0.13 \pm 0.26$
JADE	Boost. Spher. Prod.	2-decay vertices dist.	$1.46^{+0.22}_{-0.21} \pm 0.34$
TASSO	None	Dipole Moment	$1.47 \pm 0.14 \pm 0.30$
TASSO	None	Dist. to decay vertex	$1.30 \pm 0.10 \pm 0.27$
Average			1.15 ± 0.14

6 Photon Photon Collisions

In 2-γ physics, many new results have recently been obtained by PETRA experiments [62, 63,64]. In this section, however, only 2 examples will be discussed:

- Status of $\eta_c(2981)$
- Spin 1 resonance production: $f_1(1285)$ and $f_1(1420)$

6.1 Measurement of the $\gamma\gamma$ width of η_c

The measurement of the $\gamma\gamma$ width of the η_c is of particular interest, since, knowing the total hadronic width $\Gamma_{had}(\eta_c)$, one can measure the strong coupling constant α_s at the η_c mass [65]:

$$\frac{\Gamma_{had}(\eta_c)}{\Gamma_{\gamma\gamma}(\eta_c)} = f(\alpha_s^{\overline{MS}}(m_{\eta_c}^2))$$

All $\Gamma_{\gamma\gamma}(\eta_c)$ measurements are shown in Tab. 15. The lower part of the table lists the experiments which see an η_c signal. The other results are upper limits.

Recent PETRA results are from CELLO [67] and TASSO [68]. JADE [62] and CELLO [67] did not confirm the high value of $\Gamma_{\gamma\gamma}(\eta_c)$ measured by PLUTO [66]. CELLO looked for η_c in the reaction $\gamma\gamma \rightarrow \eta_c \rightarrow K^\pm K_s^0 \pi^\mp$. No signal was observed [Fig. 19], and an upper limit of $\Gamma_{\gamma\gamma}(\eta_c) < 11 KeV$ was set. TASSO investigated the decay modes

$$\eta_c \rightarrow K^\pm K_s^0 \pi^\mp$$

$$\eta_c \rightarrow \pi^+\pi^-\pi^+\pi^-$$

$$\eta_c \rightarrow K^+K^-\pi^+\pi^-$$

The mass distributions $M(K^\pm K_s^0 \pi^\mp)$ and $M(\pi^+\pi^-\pi^+\pi^-)$ [Fig. 20(a, b)] show an enhancement at the η_c mass, corresponding to a 3.5 σ signal. No signal was observed in the decay mode $\eta_c \rightarrow K^+K^-\pi^+\pi^-$ [Fig. 20(c)]. A global fit of the 3 reactions leads to the result

$$\Gamma_{\gamma\gamma}(\eta_c) = 19.9 \pm 6.1 \pm 8.6.$$

Considering the result in terms of an upper limit, TASSO obtained

$$\Gamma_{\gamma\gamma}(\eta_c) < 36 KeV (95\% CL).$$

6.2 Spin One Resonance Production

Two spin one resonances, $f_1(1285)$ and $f_1(1420)$, first observed by TPC and Mark II at PEP [69], have been confirmed by CELLO [70] and JADE [71]. The decay modes studied were:

$$\gamma\gamma \rightarrow f_1(1285) \rightarrow \pi^+\pi^-\eta$$

$$\gamma\gamma \rightarrow f_1(1420) \rightarrow K^\pm K_s^0 \pi^\mp$$

These reactions are not possible with real photons [72] ($\Gamma_{\gamma\gamma}(J=1)=0$) but can occur when one of the photons is highly virtual ($\gamma\gamma^*$ collision). The fact that the resonance structures

Table 15: Summary of the $\gamma\gamma$ width of η_c measured by different experiments. New results from CELLO, TASSO and Mark III have been added to the table of Ref 62.

Experiment	Reaction	$\Gamma_{\gamma\gamma}(\eta_c)$ [KeV]
CELLO	$\gamma\gamma \to K^{\pm}K^0_s\pi^{\mp}$	<12 (95% CL)
JADE	$\gamma\gamma \to K^{\pm}K^0_s\pi^{\mp}$	<11 (95% CL)
Mark III	$J/\psi \to \gamma\gamma\ \gamma$	<14 (95% CL)
MD-1	$e^+e^- \to e^+e^-$ Miss. Mass	<11 (90% CL)
TPC/2γ	$\gamma\gamma \to$4-prongs	< 15 (95% CL)
		>1.6 (95% CL)
PLUTO	$\gamma\gamma \to K^{\pm}K^0_s\pi^{\mp}$	28±15
Mark II	$\gamma\gamma \to K^{\pm}K^0_s\pi^{\mp}$	8±6
TASSO	$\gamma\gamma \to K^{\pm}K^0_s\pi^{\mp}$	
	$\gamma\gamma \to K^+K^-\pi^+\pi^-$	19.9±6.1±8.6
	$\gamma\gamma \to \pi^+\pi^-\pi^+\pi^-$	
TPC/2γ	$\gamma\gamma \to$4-prongs	$4.5^{+5.5}_{-3.6}$
R704	$p\bar{p} \to \gamma\gamma$	$4.3^{+3.4}_{-3.7}\pm 2.4$

only show up in tagged data is consistent with spin one production. The JADE results are shown in Fig. 21 for the $f_1(1285)$ in tagged data. Besides the $\eta\prime$ a second resonance structure at $\sim 1.28\ GeV$ is seen in the $\eta\pi^+\pi^-$ mass spectrum [Fig. 21(a)], which is correlated with the $a_0(980)$ resonance observed in the $\eta\pi^{\pm}$ mass distribution [Fig. 21(b)]. No signal was observed in untagged data [62]. The observation of the 2-body decay $f_1(1285) \to a_0^{\pm}\pi^{\mp}$ establishes the parity to be positive, since the decay $1^- \to 0^+0^-$ is forbidden. The $f_1(1285)$ signal was found to be compatible with being a $J^P = 1^+$ state with helicity 1.

The mass distribution $M(K^{\pm}K^0_s\pi^{\mp})$ shows a peak at the $f_1(1420)$ mass [Fig. 22(a)]. There is no corresponding signal in untagged data [Fig. 22(b)]. CELLO performed a Kolmogorov test to check the $J^P = 1^{\pm}$ hypotheses of the $f_1(1420)$. A probability of 58% was found for the $J^P = 1^+$ hypothesis, to be compared with 9% for $J^P = 1^-$.

The measured decay widths $\tilde{\Gamma}_{f_1(1285)}$ and $\tilde{\Gamma}_{f_1(1420)}$ are given in Tab. 16, together with the PEP results. Note that the TPC convention was used.

Table 16: Summary of $\tilde{\Gamma}$ measurements for spin 1 resonances.

Experiment	$\tilde{\Gamma}_{\gamma\gamma}(f_1(1285))$ [KeV]	$\tilde{\Gamma}_{\gamma\gamma}(f_1(1420))Br(K\bar{K}\pi)$ [KeV]
CELLO	3.6±1.1±1.2	1.5±0.5±0.4
JADE	1.8±0.3±0.4	$2.1^{+0.9}_{-0.8} \pm 0.7$
Mark II	4.7±1.25±0.85	1.6±0.7±0.3
TPC/2γ	<2.4 (90% CL)	1.3±0.5±0.3

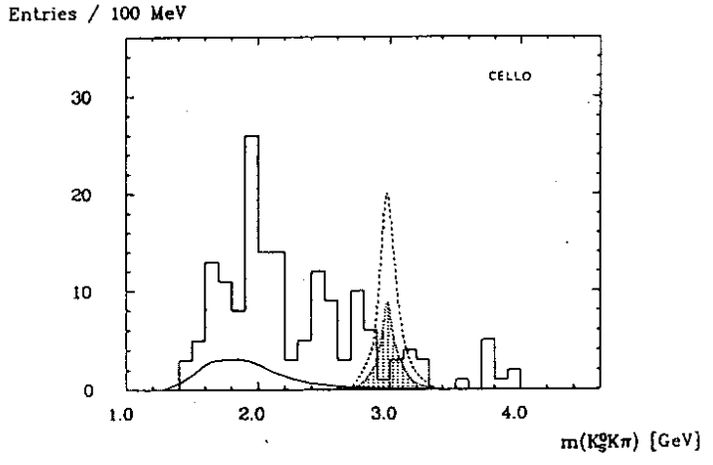

Figure 19: $K^{\pm}K^0_s\pi^{\mp}$ mass distribution from CELLO. The dashed curve shows the expectation from the PLUTO result, the dotted curve corresponds to the upper limit $\Gamma_{\gamma\gamma}(\eta_c) < 12 KeV$. The full curve is the background.

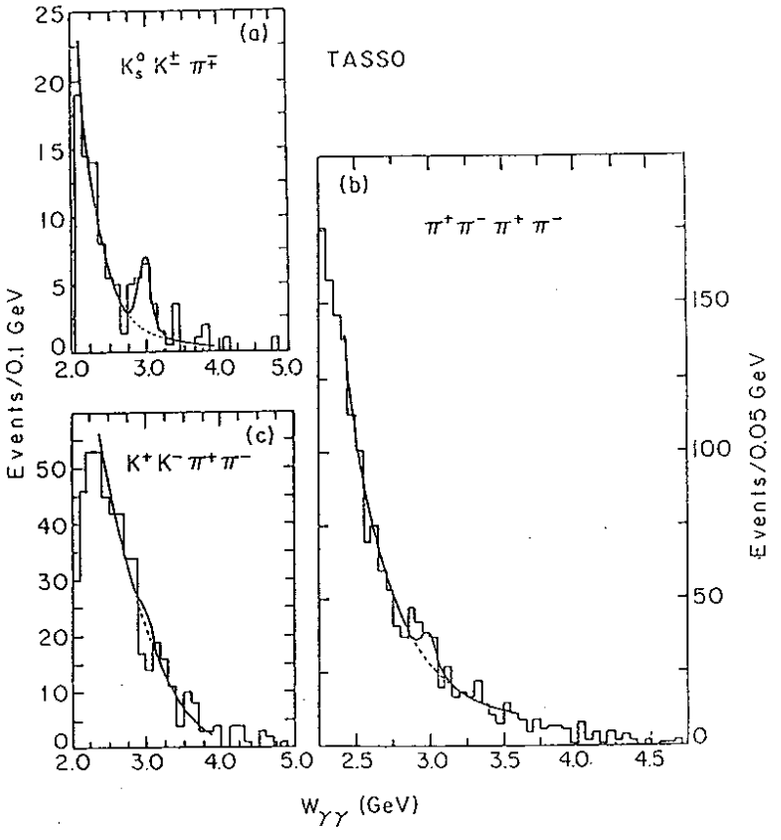

Figure 20: Mass distributions for $K^\pm K_s^0 \pi^\mp$ (a), $\pi^+\pi^-\pi^+\pi^-$ (b) and $K^+K^-\pi^+\pi^-$ (c). The full curve is the result of a global fit to the 3 reactions and the dashed curve shows the background contribution.

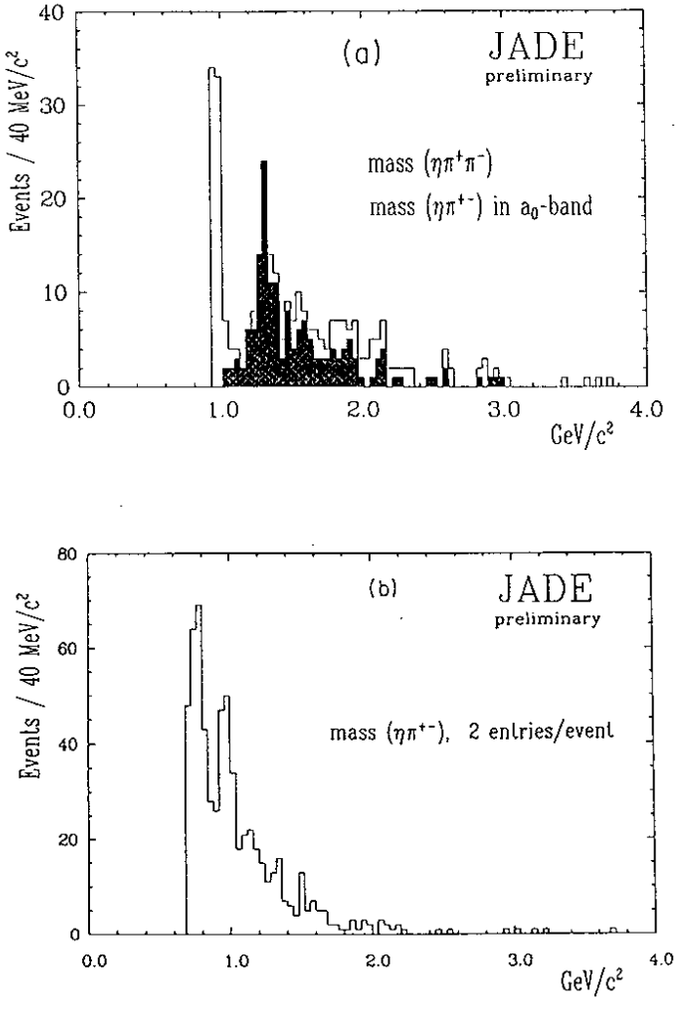

Figure 21: (a) $\eta\pi^+\pi^-$ mass spectrum in tagged data from JADE. The black histogram corresponds to the $\eta\pi^\pm$ mass spectrum in the $a_0(980)$ band defined in (b).

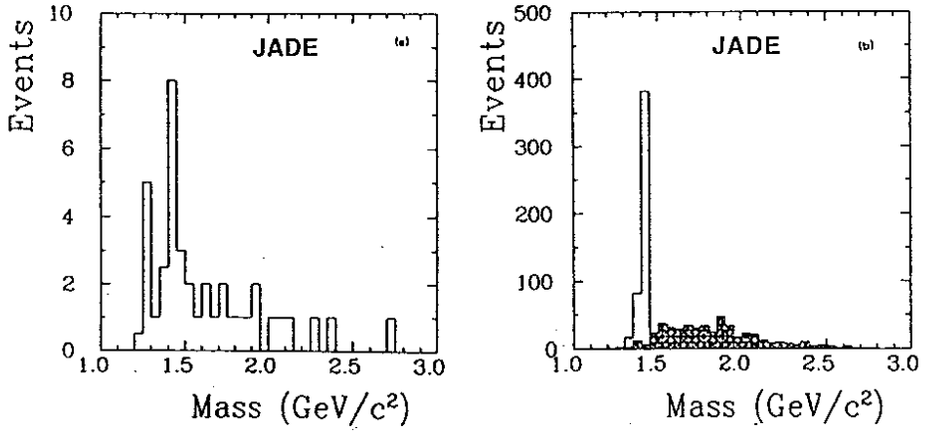

Figure 22: (a) $K^{\pm}K^{0}_{s}\pi^{\mp}$ mass distribution in tagged events from JADE.
(b) $K^{\pm}K^{0}_{s}\pi^{\mp}$ mass distribution for untagged data (shaded) and spin 0 Monte Carlo expectation (open).

Acknowledgements

I want to thank the organisers of the conference for the invitation and my colleagues at PETRA for providing me with their latest results.

References

[1] S.L. Wu, Proc. Hamburg Conference (1987), DESY Report 87-164 [8]
[2] B. Naroska, Phys. Rep. 148 (1987), 67
[3] M. Böhm, W. Hollik, Phys. Lett. 139B (1984), 213
M. Böhm, W. Hollik, H. Spieberger, Z. Phys. C27 (1985), 27
W. Hollik, Proc. XXI Rencontre de Moriond, Vol. 1 (1986) 3
[4] TASSO Collab., W. Braunschweig et al., contrib. paper to Munich Conference (#565) [9]
[5] C. Buttar, PhD Thesis, University of Glasgow (1987)
J. Mnich, PhD Thesis, RWTH Aachen (1987)
TASSO Collab., W. Braunschweig et al., DESY Report 88-059
[6] S. Elsen, Talk given at the Munich Conference
AMY Collab., Contrib. to the Munich Conference (#A492)
TOPAZ Collab., Contrib. to the Munich Conference (#504)
VENUS Collab., Contrib. to the Munich Conference (#616)
[7] CELLO Collab., H.J. Behrend et al., Contrib. to the Munich Conference (#763)
E. Deffur, PhD Thesis, RWTH Aachen (1988)
TASSO Collab., W. Braunschweig et al., Contrib. to the Munich Conference (#A207)
[8] W. Braunschweig , Talk given at the Munich Conference
[9] JADE Collab., W.Bartel et al., Phys.Lett. 146B (1984) 437
[10] CELLO Collab., H.J. Behrend et al., Contrib. to the Munich Conference (#666)
[11] JADE Collab., T. Greenshaw et al., DESY Report 88-154
[12] R. Barlow, Journal of Computational Physics 72 (1987) 202
[13] H. Albrecht et al., Phys. Lett. 192B (1987) 245
[14] TASSO Collab., W. Braunschweig et al., DESY Report 88-100
[15] R. Marshall, Contrib. to the Munich Conference (#773)
[16] A. Ali, F. Barreiro, DESY Report 88-075 and FTUM-EP-88-03
[17] W. Hofmann, Proceedings of the Hamburg conference, LBL-23922
[18] W. de Boer, SLAC-PUB-4428 (1987)
[19] JADE Collab., W. Bartel et al., Z. Phys. C 33 (1986) 23
[20] B.R. Webber, Nucl. Phys. B238 (1984) 492
[21] M. Bengtsson, T. Sjöstrand, Phys. Lett. 185B (1987) 435
T. Sjöstrand, M. Bengtsson, Computer Phys. Comm. 43 (1987) 367
[22] TASSO Collab., W. Braunschweig et al., DESY Report 88-046
[23] G. Kramer and B. Lampe, DESY Report 86-103 ; 86-119 ; 87-106
[24] CELLO Collab., H.J. Behrend et al., Contrib. to the Munich Conference (#540)
[25] N. Magnussen, PHD Thesis, Wuppertal university, WUB-DI 88-4
[26] P.M. Stevenson, Phys. Rev. D22 (1981) 2916
[27] D.W. Duke and R.G. Roberts, Phys. Rep. 120 (1985) 275
[28] Yu. Dokshitzer et al. , Phys. Lett. B78 (1978) 290
C. Basham et al. , Phys. Rev. Lett. 41 (1978) 1585 ; Phys. Rev. D19 (1979) 2018 ;
[29] A. Ali and F. Barreiro, Phys. Lett. B118 (1982) 155
D.G. Richards et al., Phys. Lett. B119 (1982) 193

[8] 1987 International Symposium on Lepton and Photon Interactions at High Energies, Hamburg, W. Germany, July 1987
[9] XXIV Int. Conference on High energy Physics, Munich, W.Germany, August 1988

[30] S.D. Ellis, Phys. Lett. B117 (1982) 333
[31] F. Csikor, Phys. Rev. D31 (1985) 1025
[32] CELLO Collab., H.J. Behrend et al., Contrib. to the Munich Conference (#685)
[33] F. Gutbrod, G. Kramer and G. Schierholz, Z. Phys. C21 (1984), 235
[34] R.K. Ellis, D.A. Ross and A.E. Terrano, Nucl. Phys. B178 (1981) 421
[35] T.D. Gottschalk and M.P. Schatz, Phys. Lett. 150B (1985) 451
[36] T. Sjöstrand, Computer Phys. Comm. 27 (1982) 243
B. Anderson et al., Phys. Rep. 97 (1983) 31
T. Sjöstrand, Computer Phys. Comm. 28 (1983) 229
[37] P. Hoyer et al.,Nucl. Phys. B161 (1979) 349
[38] A. Ali et al., Phys. Lett 93B (1979) 349
[39] PLUTO Collab., Ch. Berger et al., Z. Phys. C12 (1981), 297
[40] R.D. Field, Proc. Int. Symp. on Lepton and Photon Interactions at High Energy, Cornell (1983)
[41] CELLO Collab., H.J. Behrend et al., Contrib. to the Munich Conference (#682)
[42] T. Chandramohan and L. Clavelli, Phys. Lett. 94B (1980) 409
L. Clavelli, Phys. Lett. 85B (1979) 111
C.L. Basham et al., Phys. Rev. D19 (1979) 2018 ; D.G. Richards et al., Phys. Lett. 119B (1982) 193; A. Ali and F. Barreiro, Nucl. Phys. B236 (1984) 269
[43] CELLO Collab., H.J. Behrend et al., Phys. Lett. 183B (1987) 400
[44] G. D'Agostini, W. de Boer and G. Grindhammer, Contrib. to the Munich Conference (#764)
[45] W.J. Marciano, Phys. Rev. D29 (1984) 580
[46] S.G. Gorishny, A.L. Kataev and S.A. Larin, Phys. Lett. 212B (1988) 238
[47] F.A. Berends, G.J.H. Burgers, and W.L. van Neerven, Phys. Lett. 185B (1987) 395
[48] JADE Collab., S. Bethke et al., Phys. Lett. 213B (1988) 235
[49] CELLO Collab., H.J. Behrend et al., Phys. Lett. 114B (1982) 287
JADE Collab., W. Bartel et al., Phys. Lett. 114B (1982) 211
MARK J Collab., B. Adeva et al., Phys. Lett. 115B (1982) 345 ; Phys. Lett. 152B (1985) 439
TASSO Collab., M. Althoff et al., Phys. Lett. 122B (1983) 95
[50] CELLO Collab., H.J. Behrend et al., Phys. Lett. 193B (1987) 376
JADE Collab., W. Bartel et al., Z. Phys. 31 (1986) 359
[51] TASSO Collab., W. Braunschweig et al., Contrib. to the Munich Conference (#569)
[52] CELLO Collab., H.J. Behrend et al., DESY Report 88-052, April 1988
[53] A.D Dolgov et al., Nucl. Phys. B41 (1972) 197
E. Ma and J. Okada, Phys. Rev. Lett. 41 (1978) 287
[54] K.J.F. Gaemers et al., Phys. Rev. D19 (1979) 1605
[55] H. Wu, Ph.D. Thesis, Hamburg University (1986)
[56] ASP Collab., C. Hearty et al., Phys. Rev. Lett. 58 (1987) 1711 MAC Collab., W.T. Ford et al., Phys. Rev. D33 (1986) 3472
[57] UA1 Collab., C. Albajar et al., Phys. Lett. B198 (1987) 271
[58] CELLO, H.J. Behrend et al., Contrib. to the Munich Conference (#763)
JADE Collab., C. Kleinwort et al., DESY Report 88-155
TASSO Collab., W. Braunschweig et al., DESY Report 88-034
[59] R. Ramcke, PhD Thesis, University of Hamburg (1988)
TASSO Collab., W. Braunschweig et al., DESY Report 88-159
[60] G. Hagemann, PhD Thesis, University of Hamburg (1988)
[61] D. Muller, $c-,b-,\tau$-Lifetimes, Talk given at the Munich Conference
[62] J. Olsson, Proc. Hamburg Conference (1987) ; DESY Report 87-136
[63] H. Kolanowski and P. Zerwas, DESY Report 87-175
[64] S. Cooper, MIT-LNS-169 (1988)
[65] R. Barbieri et al., Nucl. Phys. B154 (1979) 535
K. Hagiwara et al., Nucl. Phys. B177 (1981) 461

[66] PLUTO Collab., Ch. Berger et al., Phys. Lett. 167B (1988) 120
[67] CELLO Collab., H.J. Behrend et al., DESY Report 88-149
[68] TASSO Collab., W. Braunschweig et al., DESY Report 88-050, WIS-88/15/Mar-PH
[69] Mark-II Collab., G. Gidal et al., Phys. Rev. Lett. 59 (1987) 2016 ; Phys. Rev. Lett. 59 (1987) 2012
TPC Collab., H. Aihara et al., Phys. Rev. Lett. 57 (1987) 2500 ; University of California Santa Barbara preprint UCSB-HEP-88-1
[70] CELLO Collab., M. Feindt, DESY Report 88-157
[71] JADE Collab. ,P. Hill et al., DESY Report 88-166
J. Olsson, VIIIth international workshop on 2-γ collisions, Israel (1988)
[72] L.F. Landau, Dokl. Akad. Nauk. USSR 60 (1948) 207
C.N. Yang, Phys. Rev. 77 (1950) 242